MatLLMSearch: Crystal Structure Discovery with Evolution-Guided Large Language Models

Anonymous authors
Paper under double-blind review

Abstract

Crystal structure generation is fundamental to materials science, enabling the discovery of novel materials with desired properties. While existing approaches leverage Large Language Models (LLMs) through extensive fine-tuning on materials databases, we show that pre-trained LLMs can inherently generate novel and stable crystal structures without additional fine-tuning. Our framework employs LLMs as intelligent proposal agents within an evolutionary pipeline that guides them to perform implicit crossover and mutation operations while maintaining chemical validity. We demonstrate that MatLLMSearch achieves a 78.38% metastable rate validated by machine learning interatomic potentials and 31.7% DFT-verified stability, outperforming specialized models such as CrystalTextLLM. Beyond crystal structure generation, we further demonstrate that our framework adapts to diverse materials design tasks, including crystal structure prediction and multi-objective optimization of properties such as bulk modulus, all without fine-tuning. These results establish our framework as a versatile and effective framework for consistent high-quality materials discovery, offering training-free generation of novel stable structures with reduced overhead and broader accessibility.

1 Introduction

Crystal Structure Generation (CSG) and Prediction (CSP) represent critical bottlenecks in materials discovery, requiring both chemical validity and thermodynamic stability to determine whether a material can be synthesized (Bagayoko, 2014). These tasks demand navigating an expansive chemical space while satisfying multiple constraints: three-dimensional periodicity, proper atomic coordination, charge balance, and minimized formation energy. While computational approaches have emerged as indispensable tools for accelerating materials discovery (Dunn et al., 2020; Eremin et al., 2023), developing reliable systems that effectively explore this vast and complex space remains challenging.

Recent advances in deep learning have introduced various approaches for structure prediction, from variational autoencoders to diffusion models (Flam-Shepherd and Aspuru-Guzik, 2023; Gruver et al., 2024; Jiao et al., 2024; Xie et al., 2022; Zeni et al., 2025). Meanwhile, Large Language Models (LLMs) have emerged as powerful tools for materials discovery (Achiam et al., 2023; Antunes et al., 2023; Fu et al., 2023). Prior work (Flam-Shepherd and Aspuru-Guzik, 2023) demonstrated that autoregressive models using character-level tokenization can generate valid crystal structures, and Gruver et al. (2024) showing that fine-tuning pre-trained language models like Llama (Grattafiori et al., 2024) can produce physically stable structures.

Current approaches often fine-tune LLMs on materials databases such as the Materials Project (Gruver et al., 2024), which contains only tens of thousands of structures compared to the vast space of possible stable compounds. While we propose a fundamentally different perspective: Recognizing pre-trained LLMs not as tools requiring domain-specific fine-tuning, but as intelligent agents already possessing rich embedded knowledge from vast scientific corpora. This perspective raises the question: *How can we exploit the comprehensive scientific knowledge already embedded in pre-trained LLMs to build a system that can consistently produce valid stable crystal structures?*

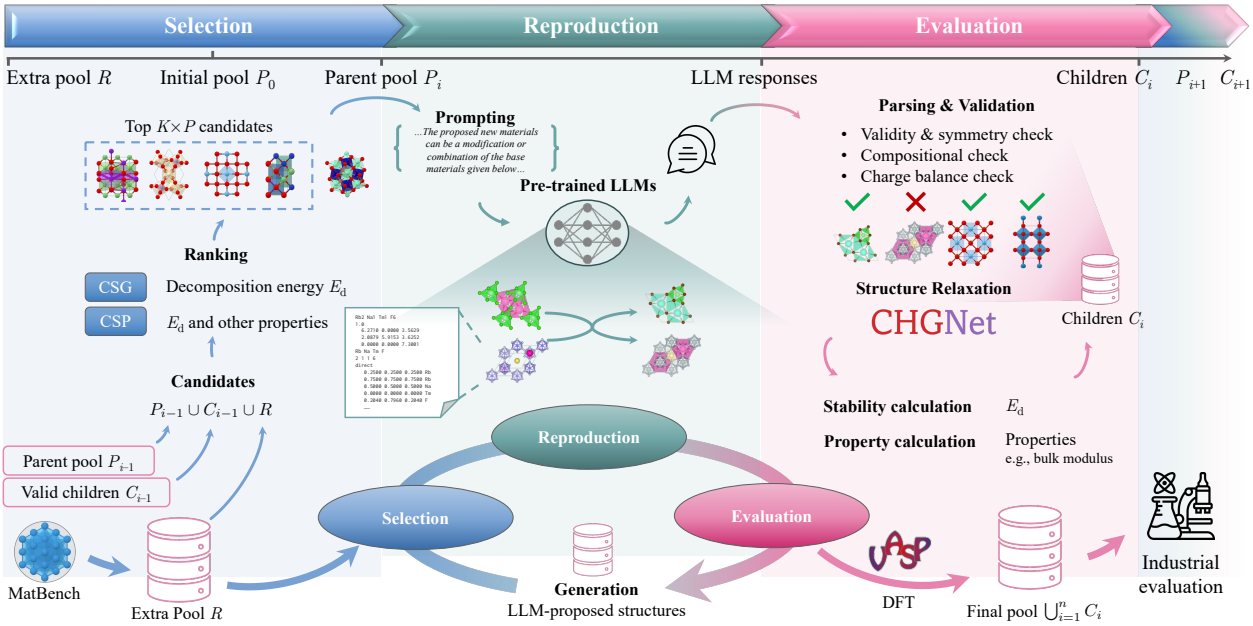

Figure 1: The workflow of MatLLMSearch for crystal structure generation. Starting from an initial population of known structures, our framework iteratively evolves new crystal structures through LLM-guided reproduction, evaluation, and selection.

Intuitively, we may directly prompt a commercial LLM to generate crystal structures. However, our ablational experiments in Section 4.4 and Appendix F across multiple configurations reveal that simple prompting fails to consistently generate valid crystal structures that are both stable and novel. These attempts often produce either copies of known structures, chemically invalid configurations, or thermodynamically unstable structures. The failure suggests that LLMs struggle to simultaneously satisfy the multiple constraints of CSG, indicating the need for a more sophisticated approach to exploit the potential of LLMs for materials discovery.

Evolutionary algorithms provide an effective framework for exploring the vast chemical space (Allahyari and Oganov, 2020; Oganov and Glass, 2006a; Wang et al., 2024). By mimicking biological evolution through iterative selection, reproduction, and mutation operations, these algorithms can gradually improve the candidates, enabling automated property-guided materials optimization. Previous evolutionary approaches to CSG and CSP rely on explicit crossover and mutation operators, such as swapping structural motifs or introducing atomic displacements. While effective, these traditional operators lack the chemical intuition to efficiently navigate the complex constraints of crystal structures, often resulting in physically implausible candidates.

Our work advances this paradigm by leveraging the rich scientific knowledge embedded in LLMs to perform chemically-informed operations within the evolutionary algorithm framework. Unlike traditional operators that manipulate structures based on predefined rules, LLMs can implicitly reason about chemical bonding patterns, structural motifs, and stability principles learned from vast scientific literature (Boiko et al., 2023; Bran et al., 2024; Guo et al., 2023). This knowledge-guided approach enables more intelligent exploration of the chemical space, potentially discovering novel structures that traditional evolutionary methods might miss due to their limited chemical knowledge.

In this work, we introduce MatLLMSearch, a novel framework that integrates the rich scientific knowledge of LLMs into the evolutionary framework for crystal structure discovery. In our proposed framework, LLMs function as intelligent proposal agents that analyze parent structures to perform implicit crossover and mutation operations, while Machine Learning Interatomic Potentials (MLIPs) evaluate the physicochemical validity of generated structures. As illustrated in Figure 1, through iterative selection, reproduction, and evaluation, MatLLMSearch progressively discovers crystal structures with desired properties.

Our experiments demonstrate that MatLLMSearch successfully generates diverse, thermodynamically stable crystal structures while maintaining crystallographic validity. The framework achieves a 76.8% metastable structure generation rate, with 31.7% of structures verified as stable through DFT calculations, surpassing the state-of-the-art fine-tuned model CrystalTextLLM (Gruver et al., 2024). Notably, this performance is achieved with minimal computational overhead, requiring only LLM inference and stability evaluation with MLIPs rather than extensive model training.

Beyond crystal structure generation, our framework demonstrates remarkable flexibility across various materials discovery tasks. Through simple modifications in prompting and reference seed structures selection, our method extends to CSP, which we validate by discovering several metastable Na_3AlCl_6 polymorphs with significantly higher stability than existing structures in the Materials Project database. Furthermore, the framework enables multi-objective optimization of properties such as bulk modulus, without requiring specialized fine-tuning. While we demonstrate results using general-purpose pre-trained LLMs, the framework could also incorporate domain-specialized fine-tuned models or alternative search algorithms, offering a computationally efficient approach to materials discovery with reduced overhead and broader accessibility.

2 Background: Computational Materials Discovery with Machine Learning

2.1 Problem Definition

Crystal Structure Generation (CSG). The objective of CSG is to learn a probability distribution $p(c, l, s)$ over crystalline materials, where $c \in \mathbb{R}^{N \times M}$ represents the chemical composition matrix for N atoms of M distinct chemical species, $l \in \mathbb{R}^6$ denotes the lattice parameters (lengths and angles), and $s \in \mathbb{R}^{N \times 3}$ defines the spatial coordinates of atoms within a periodic unit cell. Samples drawn from this distribution should ideally satisfy fundamental thermodynamic stability criteria.

Crystal Structure Prediction (CSP). CSP addresses a more constrained problem of determining stable crystal structures for a specified chemical composition. Formally, it learns a conditional probability distribution $p(s, l \mid c)$ to identify thermodynamically favorable atomic arrangements and lattice parameters given a fixed composition c. This formulation addresses the practical scenario of discovering stable polymorphs for a specified chemical formula.

Crystal Structure Design (CSD). CSD extends beyond structure prediction by incorporating property optimization and conditional generation. An example objective is finding the optimal crystal structure that maximizes a target property $h(c, l, s)$: $m^* = \text{argmax}_{c,l,s \sim p(c,l,s)}\, h(c, l, s)$, where $h : \mathbb{R}^{N \times K} \times \mathbb{R}^6 \times \mathbb{R}^{N \times 3} \to \mathbb{R}$ represents an oracle function evaluating the desired materials property. It can also be formulated as sampling from a tilted distribution $p(c, l, s)\, \exp(h(c, l, s))$ (Rafailov et al., 2024). Additional constraints can be integrated into the design process, allowing for flexible tasks such as compositional substitution (learning $p(c \mid l, s)$) and composition/structure completion (inpainting generation, learning $p(c^{\text{unknown}}, s^{\text{unknown}} \mid c^{\text{known}}, l, s^{\text{known}})$) (Dai et al., 2024).

2.2 (Meta)Stability of Materials

Among computational approaches for evaluating crystal structure stability, Density Functional Theory (DFT) is the most reliable method for predicting formation energies in solid-state materials, showing close alignment with experimental measurements (Jain et al., 2011; Sun et al., 2016). The thermodynamic stability of a structure is quantified through its decomposition energy (E_d) with respect to the convex hull of known stable phases: $E_\text{d} = E_\text{s} - \sum_i x_i E_i$, where E_s represents the total energy per atom, x_i denotes the molar fraction of the i-th competing phase, and E_i corresponds to its ground-state energy per atom. While the convex hull serves as a fixed reference, the evaluated structure s need not be part of this hull. A negative decomposition energy ($E_\text{d} < 0$) indicates a thermodynamically stable state below the convex hull, while $E_\text{d} > 0$ suggests a metastable phase with a driving force for decomposition into more stable compounds. Our main objective for CSG is to identify stable crystal structures where $E_\text{d} \leq 0$.

Given the computational intensity of DFT calculations, universal Machine Learning Interatomic Potentials (MLIPs), trained on millions of DFT calculations, have emerged as efficient and reliable proxies for structure

stability assessment. Notable among these is CHGNet (Deng et al., 2023), a Graph Neural Network (GNN)-based MLIP that uniquely incorporates magnetic moments to capture both atomic and electronic interactions. M3GNet (Chen and Ong, 2022) offers an alternative approach, implementing three-body interactions in its graph architecture for accurate structural predictions across diverse chemical spaces. Recent advances in universal MLIPs include MACE (Batatia et al., 2023), DPA-1 (Zhang et al., 2024), and JMP (Shoghi et al., 2024), which demonstrate high accuracy in predicting crystal thermodynamic stability, particularly when trained on industrial-scale datasets comprising millions of compounds and non-equilibrium atomic configurations (Barroso-Luque et al., 2024; Merchant et al., 2023; Yang et al., 2024a). In this work, we employ the pre-trained CHGNet as our universal MLIP due to its closer alignment with DFT results, using a fixed phase diagram derived from the Materials Project 2023 DFT calculations (Jain et al., 2011; Wang et al., 2021).

3 MatLLMSearch

We propose MatLLMSearch, an evolutionary workflow that leverages pre-trained LLMs to search for stable and optimized crystal structures with. In this section, we introduce three key stages of the workflow as illustrated in Figure 1: (1) **Selection**, which identifies promising candidate structures from existing pools based on stability and property metrics; (2) **Reproduction**, where the LLM generates new candidates through implicit crossover and mutations of parent structures; and (3) **Evaluation**, which assesses proposed structures for validity, stability, and target properties. The overall workflow outlined in Algorithm 1 iteratively evolves a population of crystal structures while maintaining physical constraints and optimizing desired properties.

Algorithm 1 The MatLLMSearch Framework

Require: Population size K, parent size P, reproduction size C, number of iterations N, known stable structures $\mathcal{D}$, oracle function O, extra pool $\mathcal{R}$

```
▷ Initialization
Form population P_0 by sampling K groups of P structures from D
Initialize structure collection S ← ∅
for i ← 0, 1, ···, (N − 1) do
    ▷ LLM-guided reproduction
    Generate prompts from parent structures in P_i
    Obtain children structures C_i via LLM inference and parsing
    ▷ Structure evaluation
    Relax structures C_i ← CHGNetRelax(C_i)
    Calculate decomposition energy E_d and properties
    Evaluate objective scores using oracle function O
    Update structure collection S ← S ∪ C_i
    ▷ Selection
    Form candidate pool from parents P_i, children C_i, and extra pool R
    Select top-(K × P) structures based on objective scores from the candidate pool
    Construct next parent groups P_{i+1}
Validate final structures via DFT
return cumulated structures S
```

3.1 Initialization

We first optionally sample an **extra pool** $\mathcal{R}$ of reference structures from a database of known stable structures $\mathcal{D}$. $\mathcal{R}$ is used to initialize the population and will be considered for fitting during following iterations. Our evolutionary search begins by sampling $(K \times P)$ structures from $\mathcal{D}$ to form the initial parent pairs $\mathcal{P}_0$. These structures are randomly paired into K groups of P parents each to serve as reference examples in LLM prompts. $\mathcal{R}$ can be customized to suit various design objectives, with more details and ablation studies provided in Section 4.4.

3.2 Reproduction

Genetic algorithms traditionally mimic biological evolution through explicit crossover and mutation operations (Heiles and Johnston, 2013; Johnston, 2003). In crystal structure prediction, crossover typically involves combining structural fragments from parent structures (e.g., swapping atomic positions or structural motifs), while mutation introduces random variations through predefined operations like atomic displacement, lattice transformation, or element substitution (Curtis et al., 2018; Kadan et al., 2023). While effective, these rigid operators can limit the exploration of the complex crystal structure space. In MatLLMSearch, we explore the flexibility of LLMs for structure reproduction. Through prompt-based guidance, we ask LLMs to perform implicit crossover and mutation by analyzing and combining structural information from parent materials. Specifically, LLMs are instructed to "modify or combine the base materials", while maintaining chemical validity and enhancing target properties. This approach allows LLMs to freely and simultaneously introduce variations across multiple structural aspects, including atomic positions, lattice parameters, and element substitutions, or even generate completely new structures functionally relevant to parent structures.

3.3 Evaluation

Our evaluation pipeline consists of two stages:

- **Rule-based validation** ensures structural integrity by verifying three-dimensional periodicity, physical connectivity (interatomic distances between 0.6-1.3 times the sum of atomic radii), and chemical validity through charge balance analysis.
- **Stability and property evaluation** begins with structure relaxation using CHGNet. We quantify thermodynamic stability through decomposition energy E_{d} calculated as the distance to the Materials Project convex hull. Notably, we observe that LLM-proposed structures typically require minimal relaxation, with 61.1% of structures exhibiting small energy changes ($|\Delta E| < 0.5$ eV/atom) during this process (detailed in Appendix H), indicating their initial stability. For stability-focused optimization, we quantify thermodynamic stability through the decomposition energy E_{d} using CHGNet, calculated as the distance to the convex hull from the Materials Project database (version `2023-02-07-ppd-mp`). For multi-objective optimization, additional properties such as bulk modulus can be evaluated. These quantitative scores then guide the selection process for subsequent generations, allowing our framework to flexibly adapt to different design goals.

3.4 Selection

Last, the selection stage evolves a population of candidate structures that meet the optimization objectives, such as thermodynamic stability or other desired physical properties. For each iteration i, we construct a new parent pool $\mathcal{P}_{i+1}$ of the same size ($K \times P$) by selecting top-ranked candidates from three sources: the current parent pool ($\mathcal{P}_i$), newly generated children structures ($\mathcal{C}_i$), and an optional extra pool ($\mathcal{R}$) to improve diversity. Candidates in $\mathcal{P}_i \cup \mathcal{C}_i \cup \mathcal{R}$ are ranked according to optimization objectives, either single-objective (e.g., E_{d} for stability) or multi-objective criteria (e.g., alternating between different properties).

3.5 Final DFT Verification

After completing all evolutionary iterations, we collect the cumulated children structures $\mathcal{S} = \bigcup_i \mathcal{C}_i$ for final validation using DFT. To save computational cost, we focus on meta-stable structures with CHGNet-predicted decomposition energy $E_d < 0.1$ eV/atom. DFT calculations are performed using VASP 6 in the Generalized Gradient Approximation (GGA) with PBE functional (Perdew et al., 1996), using the projector-augmented wave method (Kresse and Furthmüller, 1996; Kresse and Joubert, 1999). We employed a plane-wave basis set with an energy cutoff of 520 eV and a k-point mesh of 1,000 per reciprocal atom (Jain et al., 2013). The calculations converged to 10^{-6} eV in total energy for electronic self-consistent field cycles and 0.02 eV/Å in interatomic forces for the ionic steps. The computational settings are consistent with MPGGARelaxSet and MPGGAStaticSet (Jain et al., 2011).

Model	f-ele in Parents[†]	Validity		Metastability			Stability[‡]	
		Structural	Composition	M3GNet	CHGNet		DFT	
				$E_d < 0.1$	$E_d < 0.1$	$E_d < 0.03$	w/ f-ele	w/o f-ele[§]
CDVAE*	—	100.0%	86.7%	28.8%	—	—	5.4%	—
CrystalTextLLM-7B*	—	96.4%	93.3%	35.0%	—	—	8.7%	—
CrystalTextLLM-13B*	—	95.5%	92.4%	38.0%	—	—	14.4%	—
CrystalTextLLM-70B*	—	99.6%	95.4%	49.8%	—	—	10.6%	—
MatLLMSearch (Llama 3.1-70B)	✓	100.0%	79.4%	81.1%	76.8%	56.5%	31.7%	14.0%
	✗	100.0%	89.0%	81.9%	78.4%	54.8%	27.0%	24.6%

Table 1: Performance comparison of crystal structure generation. Metastability is first assessed using surrogate models, where we report both M3GNet and CHGNet results for fair comparison with baselines CDVAE and CrystalTextLLM (which use M3GNet). *Results taken from the original papers. [†]Indicates whether f-electron elements are excluded in parent structures (not applicable to CDVAE and CrystalTextLLM as they are trained on data including f-electron elements). [‡]The stable fraction represents the percentage of DFT-verified stable structures ($E_d < 0.0$ eV/atom) over structures predicted to be metastable ($E_d < 0.1$ eV/atom) by respective surrogate models (M3GNet for CDVAE and CrystalTextLLM, CHGNet for ours, with CHGNet being more rigorous as evidenced by lower metastability rates). [§]We exclude structures containing f-electron in DFT verification while keeping the denominator as all metastable structures.

4 Experiments

4.1 Experimental Settings

We use Llama 3.1 (70B) (Grattafiori et al., 2024) as the base LLM. We set temperature to 0.95 to balance creativity and reliability. All experiments use parent size $P = 2$, reproduction size $C = 5$, and $N = 10$ iterations, with population size $K = 100$ unless otherwise specified. Crystal structures are represented in POSCAR format with 12 decimal digits.

For initialization, we use the MatBench dataset (Dunn et al., 2020) as the known stable structure set $\mathcal{D}$. We sample some known stable structures from $\mathcal{D}$ to form the initial generation and fill the parents during each iteration. These samples are chosen based on their CHGNet-predicted decomposition energy or the properties to be optimized. Detailed ablation studies regarding this selection policy are provided in Appendix A.

4.2 Main Experimental Results

In this section, we evaluate our proposed pipeline on progressively more challenging tasks, from crystal structure generation through design to crystal structure prediction.

Crystal structure generation. We first evaluate the ability of our framework to generate stable crystal structures by optimizing decomposition energy E_d as the sole objective. The LLM prompting template is detailed in Appendix C.

The generation results are reported in Table 1. Following previous work (Gruver et al., 2024; Xie et al., 2022), we report structural and compositional validity, which assess non-overlapping atomic radii and charge neutrality respectively. Metastability is evaluated using both CHGNet and M3GNet as surrogate models, measuring the percentage of structures with decomposition energies below 0.1 eV/atom and 0.03 eV/atom thresholds. Structures identified as metastable ($E_d < 0.1$ eV/atom) by CHGNet undergo further DFT calculations for stability assessment.

We compare our model against two baseline models CDVAE (Xie et al., 2022) and CrystalTextLLM (Gruver et al., 2024). Among 1,479 generated structures, 76.8% and 81.1% are metastable based on CHGNet and M3GNet evaluations respectively, outperforming the 49.8% metastability rate by M3GNet of the state-of-the-art CrystalTextLLM 70B model, which has a comparable model size to our base model. Under rigorous DFT validation, 31.7% of the metastable structures remain stable, substantially improving the 10.6% stability rate from CrystalTextLLM 70B.

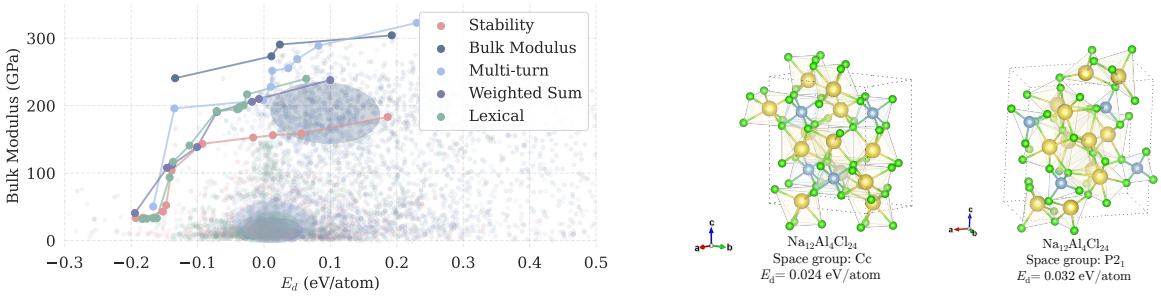

(a) Pareto frontiers

(b) CSP Examples

Figure 2: (a) Pareto frontiers of bulk modulus versus decomposition energy (E_d) for structures optimized towards stability, bulk modulus and multi-objective (multi-turn). Ellipses indicate regions of highest structure density. (b) Examples of predicted crystal structures with composition Na_3AlCl_6.

However, structures containing f-electron elements (actinides and lanthanides, abbreviated as f-ele) challenge stability prediction with their strongly correlated electron interactions, which may not be adequately captured by DFT approaches under GGA and Hubbard U corrections (Ani). These structures consistently yield lower decomposition energies (E_d), creating a potential computational shortcut. To assess this effect, we report the percentage of stable structures without f-ele (denoted as "w/o f-ele") among the metastable structures. By excluding f-electron structures from parent selection (marked with ✗), we improved metastability rates to 78.4% and increased stable non-f-electron structures from 14.0% to 24.6%. This simple intervention demonstrates our framework's ability to effectively guide exploration toward diverse stable configurations, which remain unaddressed by existing methods.

While achieving better performance, our method also offers significant computational advantages. Compared to CrystalTextLLM which requires extensive fine-tuning on more than 120K structures, we achieve higher stability rates using only a few reference structures and direct LLM inference. The computational cost is primarily from structure evaluation rather than model training or fine-tuning, making our approach more accessible.

Crystal structure design. We also explore multi-objective optimization by extending our framework to balance stability with desired material properties. We demonstrate this capability by alternating between optimizing stability (E_d) and bulk modulus in each iteration. While this multi-objective setting naturally yields lower stability rates (57.1% metastable with $E_\mathrm{d} < 0.1$ eV/atom and 15.6% DFT-verified stable structures with f-electron elements) compared to stability-only optimization, it enables the discovery of structures with favorable property-stability trade-offs.

As shown in Figure 2(a), the Pareto frontiers under various optimization strategies converge in regions with high bulk modulus ($>$ 200 GPa) and metastability ($E_\mathrm{d} \leq 0.1$ eV/atom) in the stability-property space, indicating successful discovery of potentially valuable structures that balance both objectives. The regions of highest structure density, estimated using Gaussian KDE and visualized as ellipses, reveal how optimization goals affect the distribution. Prioritizing bulk modulus shifts the density distribution toward higher mechanical strength at the cost of increased decomposition energy. We provide additional discussions of multi-objective optimization strategies in Appendix D.

Crystal structure prediction. We next evaluate our framework on crystal structure prediction tasks, which aim to predict stable structure (i.e. lattice and atomic coordinates) for a given composition. As a case study, we prompt the LLM to predict polymorphs of Na_3AlCl_6. For context, the Materials Project database currently contains only one structure for this composition (`mp-1111450`, Fm$\bar{3}$m, $E_\mathrm{d} = 0.142$ eV/atom), which is significantly unstable.

During the prompting process, we apply specific structural filters to select seed structures containing only three distinct elements in a 3:1:6 ratio, matching the stoichiometry of Na_3AlCl_6. From MatBench, we identified 820 structures meeting the criteria to build the initial population. Example structures proposed

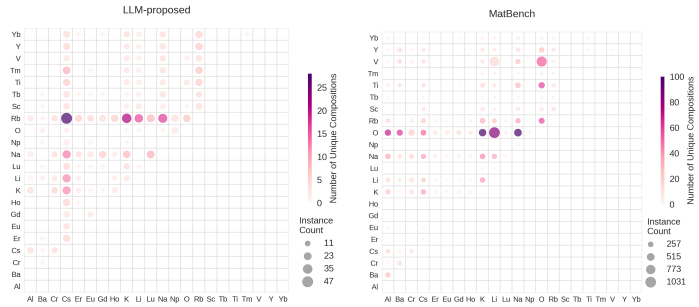

Figure 3: Element co-occurrence patterns with fluorine (F) in LLM-proposed structures (left) versus MatBench structures (right). Bubble size indicates frequency of occurrence for each element pair, while color intensity represents compositional diversity (darker indicates more unique compositions with that element pair).

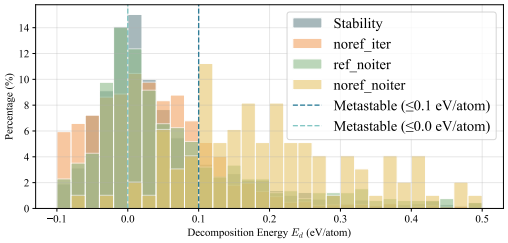

Figure 4: Decomposition energy (E_d) distribution comparison across experimental configurations. Vertical lines indicate metastable thresholds at 0.0 eV/atom (stable) and 0.1 eV/atom (metastable). Reference-guided approaches show more balanced distributions.

by the LLM for this composition are visualized in Figure 2(b), with DFT-verified decomposition energies of 0.024 and 0.032 eV/atom respectively. Although these predicted polymorphs remain metastable, their decomposition energies E_d are significantly lower than the previously reported structure in MatBench (E_d reduced by up to 83%), exemplifying the potential of our evolutionary pipeline for CSP applications. We provide more successful structure prediction demonstrations including Ag_6O_2, Bi_2F_8, etc. in the Appendix K.

4.3 CSG Quality Evaluation Metrics

4.3.1 Structural and Compositional Diversity

To better understand the effectiveness of our MatLLMSearch, we analyze the diversity of generated structures and evaluate different prompting strategies, with and without fine-tuning. Additional ablation studies on factors affecting generation performance are presented in Appendices I and J.

To evaluate the diversity of our generated structures, we analyzed their compositional and structural characteristics by comparing LLM-proposed structures and with the $K \times P$ most stable structures from MatBench that forms the initial generation. Our element co-occurrence analysis reveals high compositional diversity in the LLM-proposed structures, with even the most frequent compositions appearing only twice (approximately 0.14% of total structures). Examination of element co-occurrences with F in Figure 3 highlights the effectiveness of our evolutionary method in guiding structure generation toward stable F-based compounds, particularly with alkali metals and transition metals.

The structural diversity is further evidenced by space group distribution and stability analysis for our **Stability** configuration. The generated structures demonstrates broad structural diversity with high metastability rates across multiple space groups, confirming that our evolutionary method successfully navigates toward stable regions of chemical space while maintaining diverse structural motifs across different crystallographic symmetries. Additional diversity and novelty evaluations and analyses are provided in Appendix E.

4.3.2 Comparison with Baseline Methods

To ensure fair comparison with existing methods, we follow the same evaluation protocol proposed in FlowMM (Miller et al., 2024) and MatterGen (Zeni et al., 2025). We pre-relax all structures using CHGNet followed by density functional theory relaxation for stability verification. The results in Table 2 demonstrate that our framework maintains higher stability rate and S.U.N. (Stable, Unique, Novel) rate than the two baselines, achieving 37.59% metastability rate ($E_\mathrm{d} < 0.0$ eV/atom) and 27.65% S.U.N. rate compared to DiffCSP and FlowMM. Considering that S.U.N. depends on chosen reference sets and collapses multi-dimensional quality into counts, we position it as a supplementary signal for novelty assessment.

Section 4.3.2 (a) illustrates the key methodological difference in S.U.N. computation: while FlowMM and DiffCSP evaluate novelty against their training set, our framework compares against the full MatBench dataset (106,113 structures). Section 4.3.2(b) shows the compositional space overlap using UMAP projection of Magpie features, where generated structures (pink) show limited overlap with MatBench reference structures (blue) in compositional space.

Method	Stability Rate ($E_d < 0.0$ eV/atom, %)	S.U.N. Rate (%)
MatLLMSearch (Llama 3.1-70B)	37.59	27.65
DiffCSP	5.06	3.34
FlowMM	4.65	2.34

Table 2: Metastability and S.U.N. rate comparison. S.U.N. computed against entire MatBench-bandgap dataset.

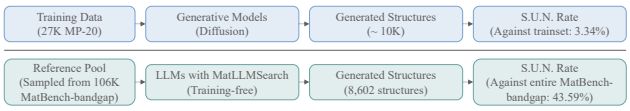

Figure 5: (a) S.U.N. methodology comparison.

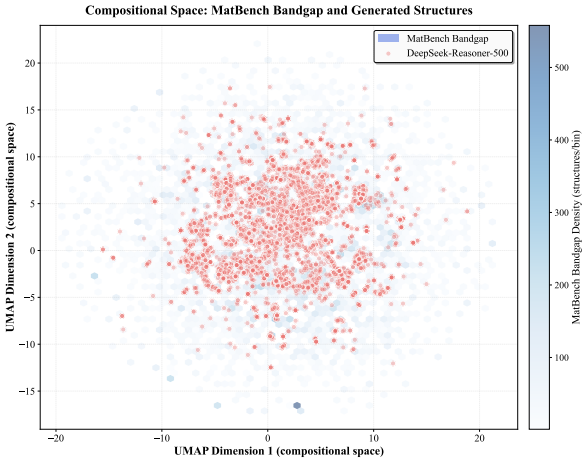

(b) Compositional space overlap (UMAP projection)

To strengthen the analysis, we also provide comprehensive evaluation covering all S.U.N. dimensions in Appendix E: DFT-calculated stability rates; metastability rates with multiple MLIPs (CHGNet, M3GNet and Orb-v3 for CSP) and space group distributions and crystal system diversity for Uniqueness; compositional and structural novelties, elemental co-occurrence pattern shifts for Novelty. We regard DFT verification as the primary validation metric, and use multi-MLIP metastability rates for baseline comparison, though they are not substitutes for first-principles DFT calculations. Further discussions on comparison fairness provided in Appendix F and additional analysis on generation time overhead and carbon footprint is provided in Appendix G.

4.4 Ablation Analysis

We evaluate four configurations to isolate the impact of reference structures and evolutionary iterations: **Stability** (full framework), **noref_iter** (evolutionary search without references), **ref_noiter** (single-iteration with references), and **noref_noiter** (zero-shot). Decomposition energy distributions (Figure 4) reveal that reference-guided approaches (**Stability**, **ref_noiter**) tightly concentrate structures near metastable thresholds, while evolutionary search alone (**noref_iter**) shows a similar but slightly dispersed distribution. In contrast, **noref_noiter** generates structures with substantially inferior metastability.

Impact of evolutionary iterations. Evolutionary iterations enable practical generation volumes: **Stability** produces 1,479 structures versus 741 for **ref_noiter**, showing higher productivity under equivalent computational budget (1,000 LLM inferences). As we investigate the distribution shift over iterations (Figure 6a), we observe that iterative optimization progressively shifts Ed distributions toward stability.

Impact of reference structures. While evolutionary search alone (**noref_iter**) achieves high metastability in later iterations, it suffers structural collapse with 88% of generated structures concentrate in triclinic space group 1 and limited exploration of other crystallographic symmetries (Figure 6c), indicating convergence to a single crystallographic motif. In contrast, reference-guided **Stability** configuration maintains comparable high metastability while distributing structures across 12 major space groups (Figure 6b). This demonstrates that reference structures prevent premature convergence while preserving thermodynamic quality.

In general, **noref_iter** achieves high metastability but diversity collapse, **ref_noiter** achieves structural diversity but limited number of structures generated, while **noref_noiter** fails on both dimensions (20.7% metastability, minimal volume). By combining reference structures with evolutionary search, **Stability**

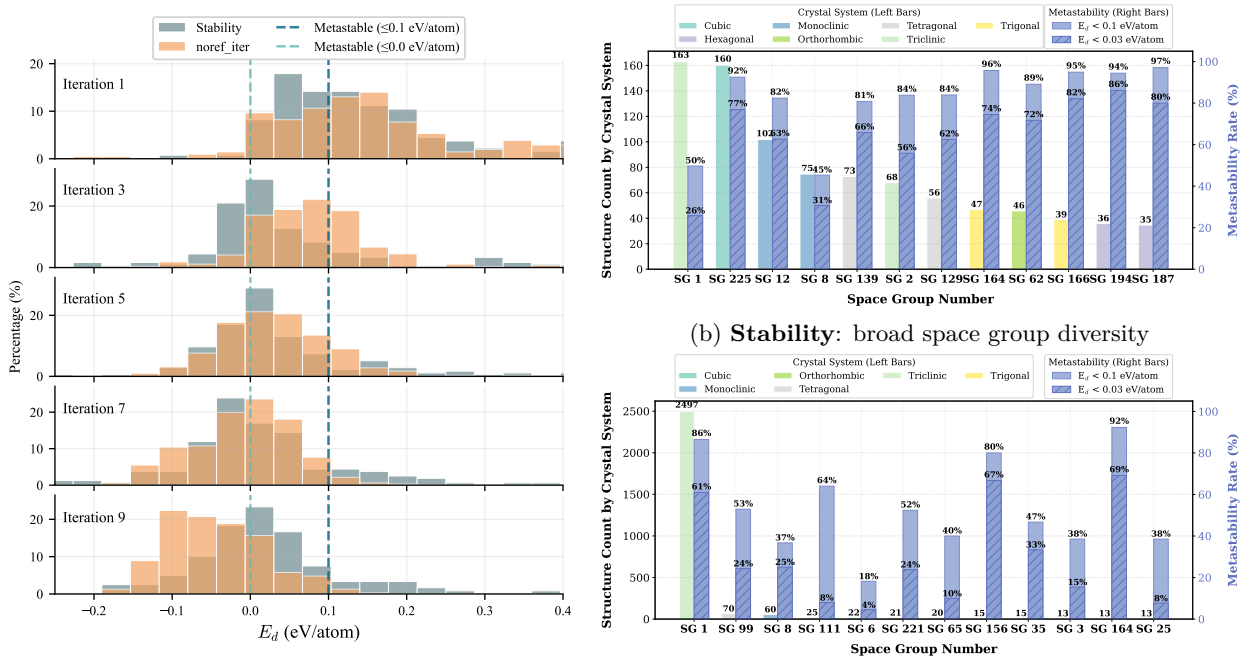

(a) E_{d} distribution evolution

(b) **Stability**: broad space group diversity

(c) **noref_iter**: limited space group diversity

Figure 6: Ablation analysis comparing reference-guided (**Stability**) vs. reference-free (**noref_iter**) generation. (a) E_{d} distributions shift toward metastable. (b) LLM-generated structures show broad space group diversity. (c) Structures show comparable metastability but limited space group diversity when generated without references.

simultaneously achieves high metastability, balanced structural diversity, and practical generation scale. Additional analysis including novelty metrics, model scaling effects, and fine-tuning comparisons appears in Appendix F.

5 Related Work

5.1 Language Models for Materials Science

The increasing capabilities of LLMs have prompted materials science community to explore their potential for understanding and predicting material properties (Jablonka et al., 2023). Benchmarking studies (Rubungo et al., 2024) also suggest that fine-tuning LLMs over specific materials datasets can lead to comparable or better performance than specialized graph neural networks.

Recent autoregressive approaches has developed along two main paths. First is to train from scratch. Flam-Shepherd and Aspuru-Guzik (2023) demonstrate that autoregressive models trained with character-level tokenization can generate chemically valid crystal structures by directly tokenizing CIF files into string sequences. Other approaches include Wyckoff Transformer (Kazeev et al., 2025) for symmetric crystal generation, deCIFer (Johansen et al., 2025) for crystal structure prediction from powder diffraction data, and multimodal foundation models (Moro et al., 2025) for material property prediction. Secondly, CrystalTextLLM (Gruver et al., 2024) fine-tunes a pre-trained LLM (over massive texts) on generating crystalline structures with task-specific prompts. Mat2Seq (Yan et al., 2024) converts 3D crystal structures into unique 1D sequences that preserve $SE(3)$ and periodic invariance for language model training. While these approaches produce valid structures, they sacrifice the general conversation capabilities of LLMs due to specialized training or fine-tuning on crystallographic data.Recent work also raised concerns about the scalability and reliability of LLMs for real-world materials discovery (Miret and Krishnan, 2024).

In parallel developments within molecular chemistry, MolLEO (Wang et al., 2025) successfully employs pre-trained LLMs without domain-specific fine-tuning to search for small molecules. Subsequent work (Lu et al., 2024) extended this evolutionary optimization approach to more complex transition metal chemistry using advanced base LLMs with enhanced reasoning capabilities. However, these applications benefit from natural string representations for molecules (e.g., SMILES or SELFIES), which are considerably simpler than the three-dimensional representations required for crystal structures. Our work bridges this gap by adapting the evolutionary approach to the more complex domain of crystal structures without requiring fine-tuning.

5.2 Generative Models for Materials Discovery

Besides autoregressive language models, various generative models including variational autoencoders, diffusion models, and flow models have emerged as promising solutions for crystal structure generation. Early work proposes generative crystal structures using variational autoencoders that represent crystal structures as 3D voxels (Court et al., 2020; Noh et al., 2019). CDVAE first proposes to generate crystal structures with a score-based generative (diffusion) model and optimize crystal structure properties through gradient-based optimization in the latent space (Xie et al., 2022). This approach has been extended in several directions: Jiao et al. (2024) developed Riemannian diffusion models to better handle periodic coordinates, Zeni et al. (2025) scaled the approach to encompass elements across the entire periodic table with various design criteria, and Dai et al. (2024) applied it to crystal inpainting tasks. Most recently, Miller et al. (2024); Sriram et al. (2024) introduced Riemannian flow matching models to better address periodic boundary conditions with improved performance. Space group-aware methods have further advanced this direction: CrystalFormer (Cao et al., 2024) uses space group informed transformers, while Chang et al. (2025); Puny et al. (2025) incorporate space group equivariance and conditional flow matching, respectively. Universal models for atoms (Wood et al., 2025) provide a unified framework for materials modeling. Yang et al. (2024b) explore the synergy between language and generative models by leveraging LLMs to propose chemical formulae under design constraints before feeding them to a diffusion model.

5.3 Evolutionary Algorithms in Materials Discovery

Evolutionary algorithm has also played an important role in materials discovery, especially *crystal structure prediction* (CSP), where the goal is to identify the global energy minimum for a given chemical composition (Oganov and Glass, 2006b; Wang et al., 2012). Representative methods include USPEX (Lyakhov et al., 2013; Oganov and Glass, 2006b), XtalOpt (Falls et al., 2020; Lonie and Zurek, 2011), GASP (Curtis et al., 2018), CALYPSO (Wang et al., 2012), and GAmuza (Kadan et al., 2023), which employ hand-crafted genetic operators such as symmetric crossover by swapping atomic positions while preserving one parent's space group and lattice mutation by perturbing crystallographic parameters. These methods have successfully predicted stable phases for systems including gamma-boron (Oganov et al., 2009), high-pressure sodium compounds (Ma et al., 2009), and metal hydrides (Peng et al., 2017). More recent approaches integrate machine learning to accelerate CSP, including active learning by MAISE (Balachandran et al., 2016), graph-based structure decomposition by MAGUS (Wang et al., 2023), and Bayesian optimization methods like GOFEE (Jennings et al., 2019) and CrySPY (Yamashita et al., 2018; 2021). We summarizes key characteristics of established evolutionary CSP methods in Table 3. Recent benchmarks (Duval et al., 2025) and reviews (Handoko and Made, 2025) provide broader context on the landscape of generative models for materials discovery.

6 Conclusion

In this paper, we present an evolutionary workflow for computational materials discovery, encompassing crystal structure generation, prediction, and objective-based optimization. We demonstrate that a pre-trained LLM trained on general text can identify a higher proportion of (meta)stable materials compared to state-of-the-art generative models specifically trained on materials datasets. These findings suggest that LLMs inherently function as effective crystal structure generators, with both compositional and structural information naturally embedded within their text inference capabilities. In conclusion, our method complements existing structure discovery techniques by providing refined optimization capabilities while maintaining versatility in addressing various optimization objectives, offering an efficient approach for high-throughput materials discovery.

Table 3: Comparison of evolutionary crystal structure prediction methods.

Method	Year	Category	Genetic Operators	Key Innovation
USPEX (Lyakhov et al., 2013; Oganov and Glass, 2006b)	2006	Classical EA	Symmetric crossover, lattice mutation	Pioneering evolutionary CSP with heredity operators
XtalOpt (Falls et al., 2020; Lonie and Zurek, 2011)	2011	Classical EA	Multiple crossover schemes	Flexible operator combinations
GASP (Curtis et al., 2018)	2015	Classical EA	Crossover, mutation, permutation	Python framework for alloys
CALYPSO (Wang et al., 2012)	2010	Classical EA	PSO-inspired operators	Particle swarm integration
MAISE (Balachandran et al., 2016)	2019	ML-Enhanced	Classical + ML screening	10-100× speedup via active learning
MAGUS (Wang et al., 2023)	2023	ML-Enhanced	Graph-decomposed operators	On-the-fly ML + graph theory
GOFEE (Jennings et al., 2019)	2019	Bayesian Opt	Gaussian process-guided	Surrogate-based convergence
CrySPY (Yamashita et al., 2021)	2021	Bayesian Opt	Modular EA + BO	Flexible multi-method framework
MatLLMSearch	2024	**LLM-Guided**	**Implicit mutation and crossover in LLM generation**	**EA + LLM for CSG, CSP, and CSD**

Looking forward, a natural extension of this work would be synthesis prediction based on the evolutionary method. Improved machine learning interatomic potentials will complement this process, as discussed in Appendix L. Such development would benefit from integration with high-quality experimental data from automated, high-throughput experiments, bridging the gap between computational predictions and experimental synthesis, which would accelerate high-throughput materials discovery.

Limitations and Broader Impact.

This work aims to advance machine learning and computational materials discovery by making crystal structure generation more accessible and efficient. This advancement will particularly benefit researchers who have limited computational resources, enabling scientific discovery without the need to train large ML models. Additionally, the oracle functions can be further adapted to incorporate experimental data or high-fidelity property predictors for the generated crystal structures when applying this pipeline to practical materials discovery.

References

Hubbard-corrected dft energy functionals: The lda + u description of correlated systems. 7

Josh Achiam, Steven Adler, Sandhini Agarwal, et al. GPT-4 Technical Report. *arXiv.org*, 2023. 1

Zahed Allahyari and Artem R. Oganov. Coevolutionary Search for Optimal Materials in the Space of All Possible Compounds. *npj Comput. Mater.*, 2020. 2

Luis M. Antunes, Keith T. Butler, and Ricardo Grau-Crespo. Crystal Structure Generation with Autoregressive Large Language Modeling. *Nat. Commun.*, 2023. 1

Diola Bagayoko. Understanding Density Functional Theory (DFT) and Completing It in Practice. *AIP Adv.*, 2014. 1

Prasanna V Balachandran, Dezhen Xue, et al. Adaptive strategies for materials design using uncertainties. *Scientific Reports*, 6:19660, January 2016. URL https://doi.org/10.1038/srep19660. 11, 12

Luis Barroso-Luque, Muhammed Shuaibi, Xiang Fu, et al. Open Materials 2024 (OMAT24) Inorganic Materials Dataset and Models. *arXiv.org*, 2024. 4, 31

Ilyes Batatia, Philipp Benner, Yuan Chiang, et al. A Foundation Model for Atomistic Materials Chemistry. *arXiv.org*, 2023. 4, 31

Simon Batzner, Albert Musaelian, Lixin Sun, et al. E(3)-Equivariant Graph Neural Networks for Data-Efficient and Accurate Interatomic Potentials. *Nat. Commun.*, 2022. 30

Erik Bitzek, Pekka Koskinen, Franz Gähler, et al. Structural Relaxation Made Simple. *Phys. Rev. Lett.*, 2006. 31

Daniil A. Boiko, Robert MacKnight, Ben Kline, and Gabe Gomes. Autonomous Chemical Research with Large Language Models. *Nature*, 624(7992):570–578, December 2023. 2

Andres M. Bran, Sam Cox, Oliver Schilter, Carlo Baldassari, Andrew D. White, and Philippe Schwaller. Augmenting Large Language Models with Chemistry Tools. *Nat. Mach. Intell.*, 2024. 2

Zhendong Cao, Xiaoshan Luo, Jian Lv, and Lei Wang. Space group informed transformer for crystalline materials generation, 2024. URL https://arxiv.org/abs/2403.15734. 11

Rees Chang, Angela Pak, Alex Guerra, et al. Space group equivariant crystal diffusion, 2025. URL https://arxiv.org/abs/2505.10994. 11

Chi Chen and Shyue Ong. A Universal Graph Deep Learning Interatomic Potential for the Periodic Table. *Nat. Comput. Sci.*, 2022. 4, 31

Bingqing Cheng. Cartesian Atomic Cluster Expansion for Machine Learning Interatomic Potentials. *npj Comput. Mater.*, 2024. 30

Callum J. Court, Batuhan Yildirim, Apoorv Jain, et al. 3-D Inorganic Crystal Structure Generation and Property Prediction via Representation Learning. *J. Chem. Inf. Model.*, 2020. 11

Farren Curtis, Xiayue Li, Timothy Rose, et al. GAtor: A First-Principles Genetic Algorithm for Molecular Crystal Structure Prediction. *J. Chem. Theory Comput.*, 2018. 5, 11, 12

Xinzhe Dai, Peichen Zhong, Bowen Deng, et al. Inpainting Crystal Structure Generations with Score-Based Denoising. In *ICML Workshop on AI for Science*, 2024. 3, 11

Bowen Deng, Peichen Zhong, KyuJung Jun, et al. CHGNet as a Pretrained Universal Neural Network Potential for Charge-Informed Atomistic Modelling. *Nat. Mach. Intell.*, 2023. 4, 31

Yuanqi Du, Limei Wang, Dieqiao Feng, et al. A New Perspective on Building Efficient and Expressive 3D Equivariant Graph Neural Networks. *NeurIPS*, 2023a. 30

Yuanqi Du, Yingheng Wang, Yining Huang, et al. M^2Hub: Unlocking the Potential of Machine Learning for Materials Discovery. *NeurIPS*, 2023b. 30

Alexander Dunn, Qi Wang, Alex Ganose, et al. Benchmarking Materials Property Prediction Methods: The Matbench Test Set and Automatminer Reference Algorithm. *npj Comput. Mater.*, 2020. 1, 6, 18

Alexandre Duval, Siddharth Betala, Samuel P. Gleason, et al. Lemat-genbench: Bridging the gap between crystal generation and materials discovery. In *AI for Accelerated Materials Design - NeurIPS 2025*, 2025. URL https://openreview.net/forum?id=ZfPGcTfDWn. 11

Roman Eremin, Innokentiy Humonen, Alexey Kazakov, et al. Graph Neural Networks for Predicting Structural Stability of Cd- and Zn-doped λ-$CsPbI_3$. *Comput. Mater. Sci.*, 2023. 1

Zackary Falls, Patrick Avery, Xiaoyu Wang, Katerina P. Hilleke, and Eva Zurek. The xtalopt evolutionary algorithm for crystal structure prediction. *Journal of Physical Chemistry. C*, 125(3), 12 2020. URL https://doi.org/10.1021/acs.jpcc.0c09531. 11, 12

Daniel Flam-Shepherd and Al'an Aspuru-Guzik. Language Models Can Generate Molecules, Materials, and Protein Binding Sites Directly in Three Dimensions as XYZ, CIF, and PDB Files. *arXiv.org*, 2023. 1, 10, 27

Nihang Fu, Lai Wei, Yuqi Song, et al. Material Transformers: Deep Learning Language Models for Generative Materials Design. *Mach. Learn.: Sci. Technol.*, 2023. 1

Aaron Grattafiori, Abhimanyu Dubey, Abhinav Jauhri, et al. The Llama 3 Herd of Models. *arXiv.org*, 2024. 1, 6

Nate Gruver, Anuroop Sriram, Andrea Madotto, et al. Fine-Tuned Language Models Generate Stable Inorganic Materials as Text. In *ICLR*, 2024. 1, 3, 6, 10, 22, 27

Taicheng Guo, Kehan Guo, Bozhao Nan, Zhenwen Liang, Zhichun Guo, Nitesh V. Chawla, Olaf Wiest, and Xiangliang Zhang. What Can Large Language Models Do in Chemistry? A Comprehensive Benchmark on Eight Tasks. In *NeurIPS*, 2023. 2

Albertus Denny Handoko and Riko I Made. Artificial intelligence and generative models for materials discovery: A review. *World Scientific Annual Review of Functional Materials*, 2025. URL https://doi.org/10.1142/S2810922825400018. 11

Sven Heiles and Roy L. Johnston. Global Optimization of Clusters Using Electronic Structure Methods. *Int. J. Quantum Chem.*, 2013. 5

Kevin M. Jablonka, Qianxiang Ai, Alexander Al-Feghali, et al. 14 Examples of How LLMs Can Transform Materials Science and Chemistry: A Reflection on a Large Language Model Hackathon. *Digit. Discov.*, 2023. 10

Anubhav Jain, Geoffroy Hautier, Shyue P. Ong, et al. Formation Enthalpies by Mixing GGA and GGA + U Calculations. *Phys. Rev. B*, 2011. 3, 4, 5

Anubhav Jain, Shyue P. Ong, Geoffroy Hautier, et al. Commentary: The Materials Project: A Materials Genome Approach to Accelerating Materials Innovation. *APL Mater.*, 2013. 5

Nidhal Jegham, Marwan Abdelatti, Chan Young Koh, Lassad Elmoubarki, and Abdeltawab Hendawi. How hungry is ai? benchmarking energy, water, and carbon footprint of llm inference, 2025. URL https://arxiv.org/abs/2505.09598. 26

Paul C. Jennings, Steen Lysgaard, Jens Strabo Hummelshøj, Tejs Vegge, and Thomas Bligaard. Genetic algorithms for computational materials discovery accelerated by machine learning. *npj Computational Materials*, 5(1), 4 2019. URL https://doi.org/10.1038/s41524-019-0181-4. 11, 12

Rui Jiao, Wenbing Huang, Peijia Lin, et al. Crystal Structure Prediction by Joint Equivariant Diffusion. *NeurIPS*, 2024. 1, 11, 25, 27

Frederik Lizak Johansen, Ulrik Friis-Jensen, et al. decifer: Crystal structure prediction from powder diffraction data using autoregressive language models, 2025. URL https://arxiv.org/abs/2502.02189. 10

Roy L. Johnston. Evolving Better Nanoparticles: Genetic Algorithms for Optimising Cluster Geometries. *Dalton Trans.*, 2003. 5

Amit Kadan, Kevin Ryczko, Andrew Wildman, et al. Accelerated Organic Crystal Structure Prediction with Genetic Algorithms and Machine Learning. *J. Chem. Theory Comput.*, 2023. URL https://doi.org/10.1021/acs.jctc.3c00853. 5, 11

Nikita Kazeev, Wei Nong, Ignat Romanov, et al. Wyckoff transformer: Generation of symmetric crystals. In *Forty-second International Conference on Machine Learning*, 2025. URL https://openreview.net/forum?id=eFHfRQRjJo. 10

G. Kresse and J. Furthmüller. Efficient Iterative Schemes for Ab Initio Total-Energy Calculations Using a Plane-Wave Basis Set. *Phys. Rev. B*, 1996. 5

G. Kresse and D. Joubert. From Ultrasoft Pseudopotentials to the Projector Augmented-Wave Method. *Phys. Rev. B*, 1999. 5

Yi-Lun Liao, Brandon Wood, Abhishek Das, et al. EquiformerV2: Improved Equivariant Transformer for Scaling to Higher-Degree Representations. In *ICLR*, 2024. 30

David C Lonie and Eva Zurek. Xtalopt: An open-source evolutionary algorithm for crystal structure prediction. *Computer Physics Communications*, 182(2):372–387, February 2011. URL https://doi.org/10.1016/j.cpc.2010.07.048. 11, 12

Jon L'opez-Zorrilla, Xabier M. Aretxabaleta, In Won Yeu, et al. ænet-PyTorch: A GPU-Supported Implementation for Machine Learning Atomic Potentials Training. *J. Chem. Phys.*, 2023. 30

Jieyu Lu, Zhangde Song, Qiyuan Zhao, et al. Generative Design of Functional Metal Complexes Utilizing the Internal Knowledge of Large Language Models. *arXiv.org*, 2024. 11

Andriy O Lyakhov, Artem R Oganov, Harold T Stokes, and Qiang Zhu. New developments in evolutionary structure prediction algorithm uspex. *Computer Physics Communications*, 184(4):1172–1182, April 2013. URL https://doi.org/10.1016/j.cpc.2012.12.009. 11, 12

Yanming Ma, Mikhail Eremets, Artem R Oganov, et al. Transparent dense sodium. *Nature*, 458(7235):182–5, March 2009. URL https://doi.org/10.1038/nature07786. 11

Amil Merchant, Simon Batzner, Samuel Schoenholz, et al. Scaling Deep Learning for Materials Discovery. *Nature*, 2023. 4, 31

Benjamin Kurt Miller, Ricky T. Q. Chen, Anuroop Sriram, and Brandon M Wood. FlowMM: Generating materials with riemannian flow matching. In *Forty-first International Conference on Machine Learning*, 2024. URL https://openreview.net/forum?id=W4pB7VbzZI. 8, 11

Santiago Miret and N M Anoop Krishnan. Are llms ready for real-world materials discovery?, 2024. URL https://arxiv.org/abs/2402.05200. 10

Viggo Moro, Charlotte Loh, Rumen Dangovski, et al. Multimodal foundation models for material property prediction and discovery. 2025. URL https://doi.org/10.1016/j.newton.2025.100016. 10

Juhwan Noh, Jaehoon Kim, Helge S. Stein, et al. Inverse Design of Solid-State Materials via a Continuous Representation. *Matter*, 2019. 11

Artem Oganov and Colin Glass. Crystal structure prediction using ab initio evolutionary techniques: Principles and applications. *The Journal of chemical physics*, 124:244704, 07 2006a. doi: 10.1063/1.2210932. 2

Artem R Oganov and Colin W Glass. Crystal structure prediction using ab initio evolutionary techniques: Principles and applications. *The Journal of Chemical Physics*, 2006b. URL https://doi.org/10.1063/1.2210932. 11, 12

Artem R Oganov, Jiuhua Chen, Carlo Gatti, et al. Ionic high-pressure form of elemental boron. *Nature*, 457 (7231):863–7, February 2009. URL https://doi.org/10.1038/nature07736. 11

Yutack Park, Jaesun Kim, Seungwoo Hwang, et al. Scalable Parallel Algorithm for Graph Neural Network Interatomic Potentials in Molecular Dynamics Simulations. *J. Chem. Theory Comput.*, 2024. 31

Max Peeperkorn, Tom Kouwenhoven, Daniel G. Brown, et al. Is Temperature the Creativity Parameter of Large Language Models? In *ICCC*, 2024. 29

Feng Peng, Ying Sun, Chris J Pickard, Richard J Needs, Qi Wu, and Yanming Ma. Hydrogen clathrate structures in rare earth hydrides at high pressures: Possible route to room-temperature superconductivity. *Physical Review Letters*, 119(10):107001, September 2017. URL https://doi.org/10.1103/PhysRevLett.119.107001. 11

John P. Perdew, Kieron Burke, and Matthias Ernzerhof. Generalized Gradient Approximation Made Simple. *Phys. Rev. Lett.*, 1996. 5

Omri Puny, Yaron Lipman, and Benjamin Kurt Miller. Space group conditional flow matching, 2025. URL https://arxiv.org/abs/2509.23822. 11

Rafael Rafailov, Archit Sharma, Eric Mitchell, et al. Direct Preference Optimization: Your Language Model Is Secretly a Reward Model. *NeurIPS*, 2024. 3

Benjamin Rhodes, Sander Vandenhaute, Vaidotas Šimkus, James Gin, Jonathan Godwin, Tim Duignan, and Mark Neumann. Orb-v3: atomistic simulation at scale, 2025. URL https://arxiv.org/abs/2504.06231. 30

Andre N. Rubungo, Kangming Li, Jason Hattrick-Simpers, et al. LLM4Mat-Bench: Benchmarking Large Language Models for Materials Property Prediction. *arXiv.org*, 2024. 10

Nima Shoghi, Adeesh Kolluru, John R. Kitchin, et al. From Molecules to Materials: Pre-Training Large Generalizable Models for Atomic Property Prediction. In *ICLR*, 2024. 4, 31

Anuroop Sriram, Benjamin K. Miller, Ricky T. Q. Chen, et al. FlowLLM: Flow Matching for Material Generation with Large Language Models as Base Distributions. In *NeurIPS*, 2024. 11, 27

Wenhao Sun, Stephen T. Dacek, Shyue P. Ong, et al. The Thermodynamic Scale of Inorganic Crystalline Metastability. *Sci. Adv.*, 2016. 3

Amanda Wang, Ryan Kingsbury, Matthew McDermott, et al. A Framework for Quantifying Uncertainty in DFT Energy Corrections. *Sci. Rep.*, 2021. 4, 31

Haorui Wang, Marta Skreta, Cher-Tian Ser, et al. Efficient evolutionary search over chemical space with large language models. 2024. URL https://arxiv.org/abs/2406.16976. 2

Haorui Wang, Marta Skreta, Cher-Tian Ser, et al. Efficient Evolutionary Search over Chemical Space with Large Language Models. In *ICLR*, 2025. 11

Junjie Wang, Hao Gao, Yu Han, et al. Magus: machine learning and graph theory assisted universal structure searcher. 10(7):nwad128, July 2023. URL https://doi.org/10.1093/nsr/nwad128. 11, 12

Yanchao Wang, Jian Lv, Li Zhu, and Yanming Ma. Calypso: A method for crystal structure prediction. *Computer Physics Communications*, 183(10):2063–2070, October 2012. 11, 12

Brandon M Wood, Misko Dzamba, Xiang Fu, et al. UMA: A family of universal models for atoms. In *The Thirty-ninth Annual Conference on Neural Information Processing Systems*, 2025. URL https://openreview.net/forum?id=SvopaNxYWt. 11

Tian Xie, Xiang Fu, Octavian-Eugen Ganea, et al. Crystal Diffusion Variational Autoencoder for Periodic Material Generation. In *ICLR*, 2022. 1, 6, 11, 22, 25, 27

Tomoki Yamashita, Nobuya Sato, Hiori Kino, Takashi Miyake, Koji Tsuda, and Tamio Oguchi. Crystal structure prediction accelerated by bayesian optimization. *Physical Review Materials*, 2(1):013803, January 2018. URL https://doi.org/10.1103/PhysRevMaterials.2.013803. 11

Tomoki Yamashita, Shinichi Kanehira, Nobuya Sato, et al. Cryspy: a crystal structure prediction tool accelerated by machine learning. *Science and Technology of Advanced Materials: Methods*, 1(1):87–97, 2021. URL https://doi.org/10.1080/27660400.2021.1943171. 11, 12

Keqiang Yan, Xiner Li, Hongyi Ling, Kenna Ashen, Carl Edwards, Raymundo Arroyave, Marinka Zitnik, Heng Ji, Xiaofeng Qian, Xiaoning Qian, and Shuiwang Ji. Invariant tokenization of crystalline materials for language model enabled generation. In *The Thirty-eighth Annual Conference on Neural Information Processing Systems*, 2024. URL https://openreview.net/forum?id=18FGRNd0wZ. 10

Han Yang, Chenxi Hu, Yichi Zhou, et al. MatterSim: A Deep Learning Atomistic Model Across Elements, Temperatures and Pressures. *arXiv.org*, 2024a. 4, 31

Sherry Yang, Simon Batzner, Ruiqi Gao, Muratahan Aykol, Alexander L Gaunt, Brendan McMorrow, Danilo Jimenez Rezende, Dale Schuurmans, Igor Mordatch, and Ekin Dogus Cubuk. Generative hierarchical materials search. In *The Thirty-eighth Annual Conference on Neural Information Processing Systems*, 2024b. URL https://openreview.net/forum?id=PsPR4NOiRC. 11

Bangchen Yin, Jiaao Wang, Weitao Du, et al. AlphaNet: Scaling Up Local Frame-Based Atomistic Foundation Model. *arXiv.org*, 2025. 30

Claudio Zeni, Robert Pinsler, Daniel Z"ugner, et al. A Generative Model for Inorganic Materials Design. *Nature*, 2025. 1, 8, 11, 23, 27

Duo Zhang, Hangrui Bi, Fu-Zhi Dai, et al. Pretraining of Attention-Based Deep Learning Potential Model for Molecular Simulation. *npj Comput. Math.*, 2024. 4, 31

Linfeng Zhang, Han Wang, Roberto Car, et al. Phase Diagram of a Deep Potential Water Model. *Phys. Rev. Lett.*, 2021. 30

Supplementary Material for **MatLLMSearch**

A Experimental Details of Population Initialization

The **Extra Pool** $\mathcal{R}$ of stable structures are sampled from known stable structures that is Matbench-bandgap dataset (Dunn et al., 2020), which consists of 106,113 crystal structures in total. To initialize the parent structures for the first iteration, we calculated the decomposition energy for each structure with CHGNet. For CSG task, we removed binary compounds and structures with high-order compositions, i.e., retaining candidate structures with 3 to 6 elements. For CSP tasks, we filtered the seed structures to find those matching a desired compositional pattern. In addition, we applied de-duplication by composition to the candidate structures. The analysis of how sampling rule of the extra pool affect the performance is provided in Section 4.4. Extra pool

B Reproducibility

The implementation of our evolutionary search pipeline is available here.

The crystal structures generated by MatLLMSearch that presented in the main results can be downloaded here. We provide structures parsed directly from LLM responses, as well as structures after CHGNet relaxation.

We also provide the generated structures and reference structures for the larger scale experiment conducted with DeepSeek-Reasoner.

C Prompt for CSG

You are an expert material scientist. Your task is to propose hypotheses for {reproduction_size} new materials with valid stable structures and compositions. No isolated or overlapped atoms are allowed.

The proposed new materials can be a modification or combination of the base materials given below.

Format requirements:

1. *Each proposed structure must be formatted in JSON with the following structure:*

```
{{
    "i":  {{
        "formula":  "composition_formula",
        "POSCAR":  "POSCAR_format_string"
    }}
}}
```

2. *Use proper JSON escaping for newlines (\n) and other special characters*

Base material structure for reference:
{reference_structures}

Your task:
1. *Generate {reproduction_size} new structure hypotheses*
2. *Each structure should be stable and physically reasonable*
3. *Format each structure exactly as shown in the input*

Output your hypotheses below:

D Additional Experiments of Crystal Structure Generation and Design

Model	f-ele in Parents	Validity		Metastability		
		Structural	Composition	M3GNet	CHGNet	
				$E_d < 0.1$	$E_d < 0.1$	$E_d < 0.03$
CDVAE	—	100.0%	86.7%	28.8%	—	—
CrystalTextLLM-7B	—	96.4%	93.3%	35.0%	—	—
CrystalTextLLM-13B	—	95.5%	92.4%	38.0%	—	—
CrystalTextLLM-70B	—	99.6%	95.4%	49.8%	—	—
MatLLMSearch (Llama 3.1-70B)	Stability	100.0%	79.4%	81.1%	76.8%	56.5%
	Bulk Modulus	100.0%	82.9%	27.0%	43.3%	8.3%
	Multi-turn	100.0%	84.1%	70.9%	57.1%	29.8%
	Weighted Sum	100.0%	88.1%	74.0%	59.8%	36.5%
	Lexical	100.0%	89.5%	84.7%	78.0%	59.9%

Table S1: Compare experimental results under various optimization goals. We explored multi-objective optimization for stability and bulk modulus in two different ways.

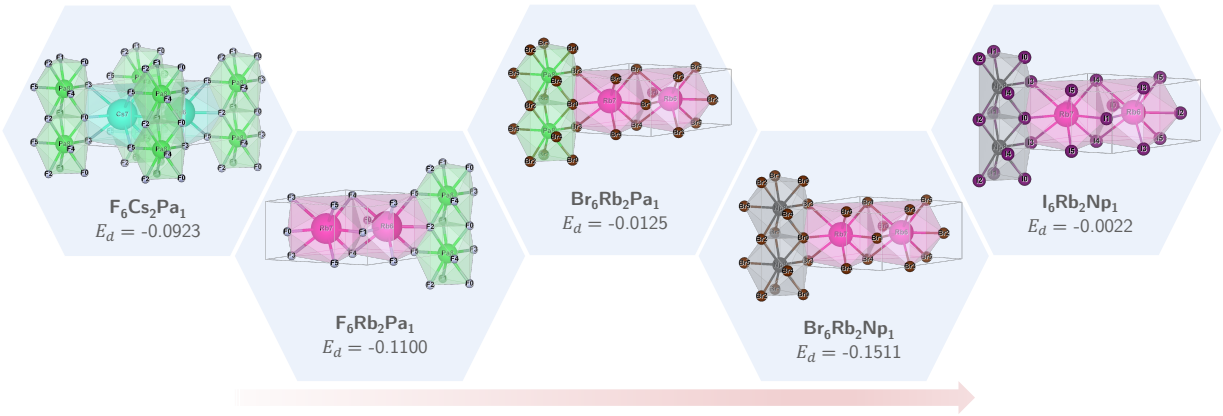

Figure S1: An example evolutionary trajectory of crystal structure generation for iteration-wise progression. The trajectory demonstrates how a structure evolve into metastable variants across iterations.

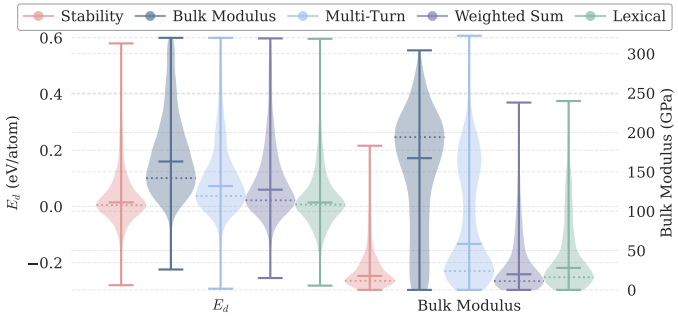

Figure S2: Comparison of optimization strategies targeting different objectives evaluated based on thermodynamic stability (decomposition energy E_d) and mechanical property (bulk modulus).

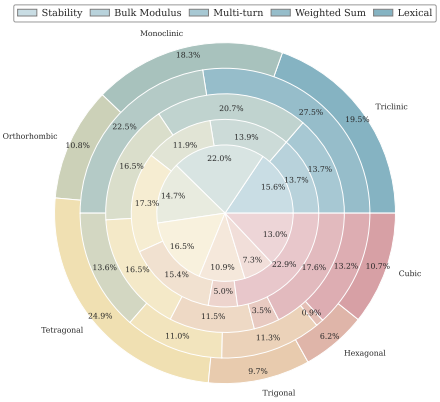

Figure S3: Crystal system distributions of generated structures under various optimization strategies. Structual diversity is preserved regardless of optimization objective.

The flexibility of our evolutionary pipeline is demonstrated by its ability to guide LLMs in proposing novel crystal structures with diverse mechanical characteristics. We evaluate model performance under five distinct optimization strategies: (1) stability-oriented optimization ("Stability"), (2) property-oriented optimization ("Bulk Modulus"), (3) alternating multi-objective optimization ("Multi-turn"), (4) normalized weighted-sum optimization ("Weighted Sum"), and (5) lexicographic optimization ("Lexical"). As shown in Table S1, all optimization strategies maintain high metastability rates for the proposed structures, demonstrating that our algorithm can optimize specific properties while maintaining high validity and stability.

Stability optimization. We visualize an example stability-oriented optimization trajectory in Figure S1.

Bulk modulus optimization. To validate the capability of MatLLMSearch for property-guided generation, we conduct single-property optimization by modifying the selection criteria from decomposition energy (E_d) to bulk modulus. In crystalline solids, bulk modulus serves as a key indicator for designing materials with enhanced mechanical hardness.

Bulk modulus values were computed using an Equation of State (EOS) workflow with the CHGNet potential. Structures are first relaxed with CHGNet to reach local energy minima. Isotropic volume perturbations were then applied to generate distorted structures. For each perturbation, a constrained ionic relaxation was performed to optimize atomic positions while fixing the cell dimensions, using a force convergence criterion of 0.1 eV/Å and a maximum of 500 optimization steps. Finally, the resulting energy-volume data were fitted to the Birch-Murnaghan EOS to extract the bulk modulus, which was then converted to GPa.

Figure S2 presents the distribution comparison of decomposition energy (E_d) and bulk modulus for structures generated under varied optimization strategies, revealing distinct performance trade-offs. The bulk modulus optimization generated more structures with larger bulk modulus values, reaching a peak density at 194 GPa compared to only 19 GPa in stability-oriented optimization. However, this enhancement comes at the cost of increased decomposition energy, with the E_d density peaks shifting from 0.0 eV/atom in stability-oriented optimization to 0.1 eV/atom in bulk modulus optimization, indicating reduced thermodynamically stability across iterations.

Bulk modulus controllability. We evaluate CSD tasks targeting specific bulk modulus values as well as maximizing, as shown in Table S2. The experiments are conducted with deepseek-reasoner for population of 10 for 5 iterations.

Table S2: Bulk modulus controllability results for CSD tasks: 1. targeting 100 GPa, 2. maximizing.

Target Bulk Modulus (GPa)	**Avg Bulk Modulus (GPa)**				
	Iter 1	**Iter 2**	**Iter 3**	**Iter 4**	**Iter 5**
100	88.5 ± 67.4	91.5 ± 42.7	89.4 ± 28.4	98.7 ± 25.5	90.9 ± 25.9
Maximize	96.1 ± 63.5	123.7 ± 40.9	149.5 ± 42.9	171.8 ± 50.8	232.6 ± 47.2

Our proposed MatLLMSearch shows **effective controllability** with the average bulk modulus converging to 98.7 GPa by iteration 4, while the maximize experiment shows continuous improvement. The results demonstrate the flexibility of our framework for various crystal structure design tasks.

Multi-objective optimization. Beyond single-objective optimization, we explored multi-objective optimization approaches to simultaneously target both thermodynamic stability and mechanical properties using two different multi-objective optimization strategies.

First we implement an alternating optimization strategy ("Multi-turn"), where the algorithm alternates between optimizing stability and property in successive iterations. Stability is optimized in the first iteration to set a foundation for property optimization. For customized multi-objective optimization, the number of iterations for each optimization goal can be adjusted. As shown in Figure S2, this method achieves balanced performance in optimizing stability and bulk modulus, with E_d centered around 0.037 eV/atom. We observe that bulk modulus distribution separates structures into groups with high mechanical strength at moderate stability versus high stability with lower mechanical strength, suggesting the inherent trade-off in crystal structure generation.

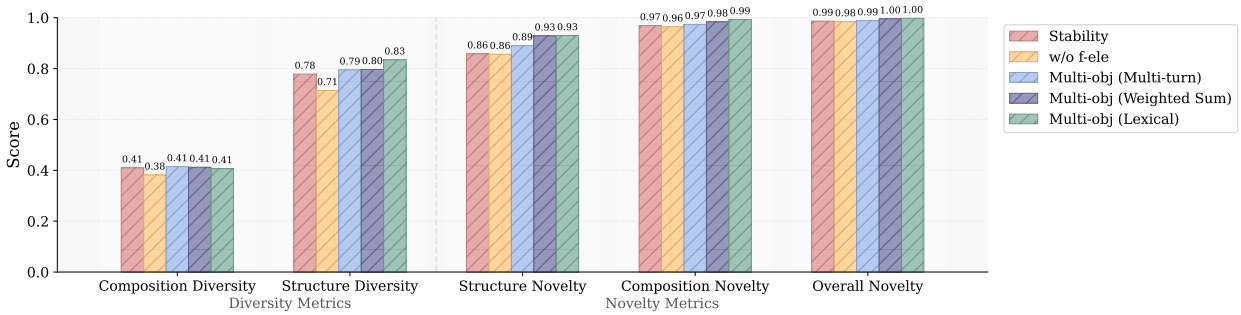

Figure S4: Diversity and novelty evaluation results for structures proposed under different experimental settings.

Then we consider a normalized weighted-sum approach that combines both objectives into a single scalar function. We apply min-max normalization to both E_d and bulk modulus values, then compute the objective as $\mathcal{J} = w_e \cdot \hat{E}_\mathrm{d} + w_b \cdot (1 - \hat{B})$, where $\hat{E}_\mathrm{d}$ and $\hat{B}$ are the normalized values, and $w_e = 0.7$, $w_b = 0.3$ are the weights. This strategy produces crystal structures with bulk modulus centered around 141 GPa and E_d centered at 0.034 eV/atom.

Then, the "Lexical" method prioritizes stability as the primary criterion, only considering bulk modulus for metastable structures ($E_\mathrm{d} < 0.03$ eV/atom). For stable structures, the weighted sum of the two objectives are then being optimized. Low stability structures are penalized to ensure that it remains the dominant factor. While single-objective stability optimization achieves the highest metastability rate of 76.8%, all multi-objective approaches maintain metastability rates above 50% while enhancing mechanical properties.

In addition, the analysis of crystal system distributions in Figure S3 indicates that our framework preserves structural diversity regardless of the optimization objective.

E Additional Evaluation on Diversity and Novelty

E.1 Diversity and Novelty Metrics.

We quantitatively evaluate the diversity and novelty of structures generated by our framework across configurations using established metrics from prior work (Gruver et al., 2024; Xie et al., 2022). Crystal diversity is measured by computing pairwise distances between their structural and compositional fingerprints. Additionally, we apply log normalization to composition diversity for 0-1 scale standardization. The novelty measures the distance between generated samples and their closest neighbors in the extra pool of reference structures. The structural distance cutoff and composition distance cutoff used for novelty calculation are 0.1 and 2 respectively. To align with previous work, all metrics are computed on structures predicted to be metastable.

The results are summarized in Figure S4. Across different optimization goals, we observe an interesting trade-off between property-specific optimization and novelty, balancing targeted enhancement against chemical space exploration. When optimizing beyond stability alone, such as targeting bulk modulus or performing multi-objective crystal structure design, we observe decreased novelty while diversity remains consistently high across all optimization goals.

While LLMs do tend to favor known stable configurations, our framework's evolutionary approach encourages the exploration of diverse structural motifs, as evidenced by the relatively uniform crystal system distributions.

E.2 On S.U.N. metric fairness.

To further assess structural diversity, we extended our evaluation with additional metrics, including the S.U.N. Rate (Stable, Unique, Novel) aligning to MatterGen and diversity and novelty regarding composition and

structure in **??**. The S.U.N. metric (Zeni et al., 2025) is convenient but limited: it collapses multi-dimensional quality into counts and depends on the chosen reference/training sets. Our MatLLMSearch is training-free; therefore, we compute S.U.N. against the entire MatBench bandgap dataset where the parent structures sampled from. Direct cross-model comparison is inherently challenging. We therefore position S.U.N. as a supplementary signal while DFT verification remaining the gold standard.

We provide comprehensive evaluation across all S.U.N. dimensions: For Stability, we report DFT-calculated stability rates and metastability rates computed with multiple MLIPs (CHGNet and M3GNet for CSG and additional Orb-v3 for CSP) providing more rigorous thermodynamic assessment than S.U.N.'s single stability threshold. For Uniqueness, we provide detailed analysis including space group distributions and crystal system diversity, offering deeper insights into the true diversity of generated structures. For Novelty, we measure compositional and structural novelties and demonstrate elemental co-occurrence pattern shifts that indicate genuine exploration of novel composition space regions. High diversity and novelty are consistently achieved by our approach under various settings.

E.3 Novelty Verification Against Materials Project and Compositional Space Analysis

To rigorously address concerns about data leakage and memorization, we performed two complementary analyses: (1) structural novelty verification against the Materials Project database (>200,000 structures) using compositional and structural matching, and (2) compositional space coverage analysis via UMAP projection of Magpie features.

Novelty Verification Methodology. We verify novelty against Materials Project using two criteria: *compositional novelty* (exact formula matching) and *structural novelty* (RMSD-based matching with pymatgen StructureMatcher: ltol=0.2, stol=0.3Å, angle_tol=5°, threshold RMSD<0.3Å). Structures are classified as *overall novel* only if both composition and structure are novel, ensuring conservative assessment. Structures with known compositions but novel crystal arrangements are identified as *novel polymorphs*, which represent scientifically valuable discoveries as polymorphs can exhibit dramatically different properties despite identical composition.

Compositional Space Coverage Analysis. Complementing the novelty verification, we visualize compositional space coverage using UMAP projection of Magpie features for MatBench (106,113 structures) and generated structures (8,602 from DeepSeek-Reasoner) and MP-20. Quantitative analysis reveals: (1) *Limited reference data memorization*: generated structures exhibit larger average distance to nearest seed compared to typical MatBench inter-structure distance, providing spatial evidence against memorization; (2) *Low-density exploration*: 47% of generated structures occupy the bottom quartile of MatBench density distribution, demonstrating substantial exploration beyond established chemical space; (3) *Spatial separation*: generated structures (pink dots) show clear spatial separation from MatBench-bandgap (blue) in the UMAP projection, with wide distribution across both high-density (validated regions) and low-density (exploratory regions) areas.

Addressing Data Leakage Concerns. We acknowledge that complete elimination of data leakage is impossible with LLMs trained on scientific corpora. However, our analysis shows the framework's novelty claims remain robust. Together, these analyses provide multi-faceted evidence against data leakage: (1) *Low database overlap*: only 23.6-30.8% compositional overlap with Materials Project across experiments; (2) *High structural novelty*: 81.5-84.4% of structures have RMSD>0.3Å from all MP structures; (3) *Low-density exploration*: 47% coverage in underexplored regions; (5) *Novel polymorph discovery*: 8-12% of structures are scientifically valuable novel arrangements of known compositions; (6) *Consistent performance across models*: similar novelty rates for Llama3-70B (69.2%) and DeepSeek-Reasoner (76.4%) demonstrate method robustness rather than model-specific memorization. Even under the conservative assumption that all 30.8% compositionally-matched structures represent memorization, 69.2% of generated structures remain fully novel—both compositionally and structurally—validated against >200,000 MP structures.

E.4 Larger Scale Experiment.

To be comparable at 10k level structures that more aligned with other baselines, we conduct a larger scale experiment with DeepSeek-Reasoner, where we use population size 500 for 10 iterations. We computed the S.U.N. rate for the generated structures against the reference structures used in our workflow. The results are presented in Table S4.

F Additional Discussion on Ablation Analysis.

F.1 Base LLM Analysis

Model Scale Effects. We evaluate the framework across different LLM configurations, including pre-trained and fine-tuned Llama 3.1 models (8B and 70B). Table S3 demonstrates that model capability significantly impacts CSG metastability. The 70B model achieves 76.8% metastability in our full framework compared to 27.7% for the 8B model, indicating that crystallographic knowledge emerges at sufficient model scale.

Base Model	Fine-Tuning?	Prompting Strategy	Metastable(%) (CHGNet)	
			$E_d < 0.1$ eV/atom	$E_d < 0.03$ eV/atom
Llama 3.1 8B	✗	Zero-shot	0.0	0.0
		MatLLMSearch	27.7	10.0
	✓(8 bit)	Zero-shot	0.0	0.0
		MatLLMSearch	45.5	22.7
Llama 3.1 70B	✗	Zero-shot	25.8	12.9
		MatLLMSearch	76.8	56.5
	✓(4 bit)	Zero-shot	13.9	2.8
		MatLLMSearch	66.0	48.0

Table S3: Meta-stability comparison of prompting strategy across models with and without fine-tuning.

Fine-tuning Integration. Fine-tuned models show substantial improvements when integrated with our evolutionary framework. The 8B fine-tuned model achieves 45.5% metastability (from 27.7% baseline), while the 4-bit quantized 70B model maintains 66.0% metastability despite compression constraints. See Table S3 for detailed results and prompting strategies. Importantly, our information value metric demonstrates that both fine-tuned and pre-trained models integrate seamlessly into the evolutionary framework, with performance scaling according to base model capability.

Generation Strategy Comparison We extend the comparison to two generation strategies: zero-shot (w/o reference structures nor evolution) and our evolutionary framework. Zero-shot approaches fail for 8B models and achieve only 25.8% metastability for 70B models. Our evolutionary framework overcomes these limitations by systematically exploring chemical space while maintaining high stability rates.

The comprehensive analysis reveals several critical insights: (1) Reference structures simultaneously accelerate convergence and promote structural diversity exploration across multiple dimensions, (2) Evolutionary iterations are essential for practical generation volumes and sustained quality optimization, (3) The synergistic combination of both components achieves optimal performance that exceeds individual contributions, (4) Our information value metric successfully captures complex trade-offs that single-dimensional metrics miss, enabling objective comparison across methodologies. These findings establish a robust evaluation framework for crystal structure generation while demonstrating the effectiveness of our evolutionary approach.

F.2 Extended Base LLM Comparison.

We evaluate MatLLMSearch with 6 LLMs across multiple model families (DeepSeek, GPT, Grok, Claude). Results in Table S4 compare against CDVAE and DiffCSP baselines.

Metrics. We report: (1) *Validity*: fraction of generated structures with proper stoichiometry and 3D periodicity; (2) *Metastability at* $E_d < 0.1$ *eV/atom evaluated with CHGNet*; (3) *Metastability at* $E_d <$

0.0 *eV/atom*; (4) *S.U.N. Rate (Structures Unique and Novel)*: fraction of generated structures that are simultaneously (a) thermodynamically stable ($E_\mathrm{d} < 0.0$ eV/atom), (b) compositionally novel (formula not in extra pool), and (c) structurally novel (structure does not match extra pool via pymatgen StructureMatcher). S.U.N. rate calculated against entire MatBench band-gap dataset as extra pool.

Table S4: Performance comparison of LLMs on MatLLMSearch crystal structure generation task. LLM models use temperature: 1.0, max tokens: 8000.

Method	**Validity** (%)	**Metastability** ($E_\mathrm{d} < 0.1$ **eV/atom, %**)	**Stability** ($E_\mathrm{d} < 0.0$ **eV/atom, %**)	**S.U.N. Rate** (%)
CDVAE (Xie et al., 2022)	86.70	28.80	–	–
DiffCSP (Jiao et al., 2024)	83.25	–	5.06	3.34
GPT-5-mini	98.45	74.60	50.05	46.24
GPT-5-chat	98.12	64.36	46.93	44.37
GPT-5	99.63	88.33	**63.22**	**55.31**
Grok-4	**99.92**	87.13	60.29	49.80
DeepSeek Reasoner	99.25	**88.90**	61.22	48.25
Claude Sonnet 4.5	99.10	78.71	50.21	38.99
Larger-Scale Experiment (population $K = 500$, 10 iterations)				
DeepSeek Reasoner	98.97	84.31	55.51	43.59

Table S5: Novelty analysis for MatLLMSearch: comparison between original experiment (Llama-3.1-70B, $K = 100$) and larger-scale experiment (DeepSeek-Reasoner, $K = 500$).

Metric	**Llama-3.1-70B** ($K = 100$)	**DeepSeek-Reasoner** ($K = 500$)
Total Structures	1,479	8,602
Compositional Novelty	1,023 (69.2%)	6,568 (76.4%)
Structural Novelty	1,205 (81.5%)	7,260 (84.4%)
Compositions in MP	456 (30.8%)	2,034 (23.6%)
Structures Matched	274 (18.5%)	1,342 (15.6%)
Novel Polymorphs	182 (12.3%)	692 (8.0%)
Composition Diversity	1,417 unique (95.8%)	8,444 unique (98.2%)

Table S6: Ablation analysis of MatLLMSearch components (Llama-3.1-70B, $K = 100$). "Ref" indicates use of reference structures, "Iter" indicates iterative evolution.

Configuration	**Overall Novelty**	**Comp. in MP (%)**	**Struct. Matched (%)**
MatLLMSearch (Ref + Iter)	69.2%	30.8%	18.5%
No Ref + Iter	**91.4%**	**8.6%**	**1.8%**
Ref + No Iter	72.6%	27.4%	16.7%
No Ref + No Iter	56.7%	43.3%	5.5%

Larger-scale Experiment. We extend the experiment to population size $K = 500$ to investigate scalability of LLM-guided evolution. Results in Table S4 show that while metastability and S.U.N. rates decrease slightly, this reflects the *exploration-exploitation trade-off* inherent to evolutionary algorithms: larger populations prioritize diversity and search space coverage over per-structure optimization. The absolute discovery count increases approximately 5 ×, demonstrating that MatLLMSearch scales effectively for high-throughput materials discovery workflows. The metastability rate still vastly exceeds diffusion baselines, confirming that LLM-guided evolution maintains thermodynamic validity even at scale.

Novelty Verification. Table S5 presents novelty analysis comparing both experiments. Both demonstrate strong evidence against memorization: (1) *Low database overlap*: Minimal compositional overlap with Materials Project's known structures, with the majority remaining compositionally novel. (2) *Novel polymorphs*: Substantial numbers of novel polymorphs represent new crystal arrangements of known compositions, demonstrating structural innovation. (3) *High diversity*: Over 95% unique compositions indicate substantial

Model	Energy (kWh / 1,000 tokens)	Total Tokens (M)	Energy (kWh)	CO_2 (kg)
claude-sonnet-4-5	0.00139	4.72	6.56	2.92
deepseek-reasoner	0.01450	8.04	116.52	51.85
gpt-5	0.00326	7.06	22.98	10.22
gpt-5-chat	0.00326	2.73	8.90	3.96
gpt-5-mini	0.00071	5.79	4.10	1.83
grok-4	0.00605	7.25	43.89	19.53

Table S8: Estimated carbon footprint for LLM API calling.

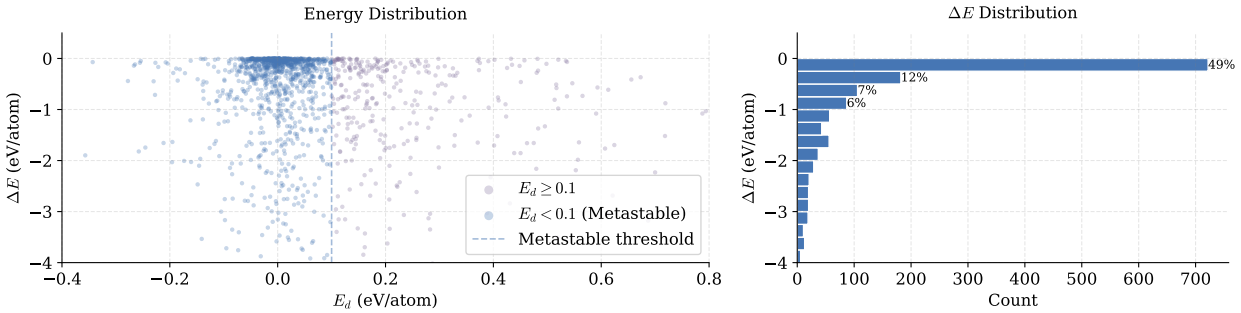

Figure S5: Distribution of energy change ΔE before/after structural relaxation and decomposition energy (E_{d}) for structures proposed by LLM, evaluated using the pretrained CHGNet.

exploration of chemical space. The larger-scale experiment achieves higher novelty metrics, suggesting that increased population size enhances exploration capabilities.

We also provide evaluated novelty against Materials Project for the ablation experiments in Table S6. The ablation experiment without reference structures achieves the highest novelty with minimal MP overlap, providing strong evidence that successful generation is not powered by memorizing existing crystal structures.

G Time and Resource Overhead

The efficiency of our method is primarily determined by the hardware resources and model size used. As reported in Table S7, with Llama-3.1-70B-Instruct running on 4 A6000 GPUs and a population size of 100, the average time to propose one valid unique structure is 62.35 seconds. In comparison, Crystal-TextLLM takes 51.6 seconds on average to propose one valid structure. Our time overhead can be further optimized with improved computational resources.

Model	Avg. Generation Time (s)	Avg. Evaluation Time (s)
70B	55.99	6.36
8B	53.40	10.80

Table S7: Time overhead comparison for different LLM model sizes.

Inference cost rationale. We report average time per successfully generated valid structure, rather than raw FLOPs, because larger models achieve higher success rates per attempt. Although a 70B model has higher per-step compute than an 8B model, its greater validity rate often yields lower cost per successful sample.

Carbon Footprint. In Table S8, we convert the total number of input and output tokens into energy and CO_2 emissions using infered energy-per-token factors (Jegham et al., 2025) to estimate the resulting emissions of LLM training and inference.

Method	Primary Format	Generative	Model	Training
CDVAE (Xie et al., 2022)	3D	Diffusion	GNN	Training
MatterGen (Zeni et al., 2025)	3D	Diffusion	GNN	Training
Flam-Shepherd and Aspuru-Guzik (2023)	3D	AR	Transformer	Training
DiffCSP (Jiao et al., 2024)	3D	Diffusion	GNN	Training
CrystalTextLLM (Gruver et al., 2024)	Text/CIF	LLM	Transformer	Fine-tuning
FlowMM (Sriram et al., 2024)	3D	Flow	GNN	Training
MatLLMSearch (Ours)	Text/CIF/POSCAR	LLM	Llama 3.1	N/A

Table S9: A collection of generative models on computational materials discovery. Training denotes if training/fine-tuning is required on materials databases.

Format	# Unique / # Total generated	$E_\mathrm{d} < 0.1$ eV/atom	$E_\mathrm{d} < 0.03$ eV/atom
POSCAR (4)	76.7%	75.4%	55.3%
POSCAR (12)	72.3%	76.8%	56.5%
CIF	75.1%	68.9%	49.5%

Table S10: Proportion of unique structures and their CHGNet-predicted metastability using different structure formats.

H Impact of Structure Relaxation

To measure the contribution of structural relaxation in our framework, we introduce a quantity ΔE to represent the energy difference after and before structural relaxation using CHGNet. Figure S5 reveals that the majority of the proposed structures proposed by LLMs exhibit a relatively small ΔE, with 61.2% showing minimal energy changes ($|\Delta E| < 0.5$ eV/atom) during relaxation. This distribution indicates that our framework generates physically meaningful structures that are already close to their local energy minima, requiring only modest refinements through relaxation.

I Impact of Structural Representation

A number of computational methods has emerged for crystal structure generation using machine learning approaches, as shown in Table S9. Most methods represent crystal structures using 3D information processed through either Graph Neural Networks (GNN) or Transformer architectures, employing various generative strategies like diffusion models or autoregressive approaches. More recently, text-based formats and Large Language Models (LLMs) have emerged as an alternative approach, signaling a promising shift in crystal structure generation and analysis techniques.

The encoding of crystallographic structures into text-based format is essential for LLM processing. We investigated the impact of different structural representation strategies on generation efficiency and performance: CIF format and POSCAR format with either 4 or 12 decimal places of precision. See Figure S6 for examples.

First, we examine the token efficiency by analyzing the MatBench dataset for token length distribution as shown in Figure S7. The distribution indicates that the POSCAR format with 4 decimal places offers the most token-efficient representation while maintaining reasonable precision, followed by the POSCAR with 12 digits and CIF format. CIF format requires more tokens than POSCAR format, given that CIF uses a more verbose structure and additional metadata.

Performance evaluation shown in Table S10 suggests that POSCAR formatting in 12 decimal places demonstrates slightly better overall performance in the rate of (meta)stability of generated structures under different criteria ($E_\mathrm{d} < 0.03$ or 0.1 eV/atom). Therefore, we employ POSCAR of 12 decimal places as a trade-off results of token efficiency and informativeness. The marginal difference across format may be attributed to the

crystallographic data exposed to the LLMs during pre-training. However, it is noteworthy that performance differences across formats remain modest, suggesting the resilience of our approach across different structural representations.

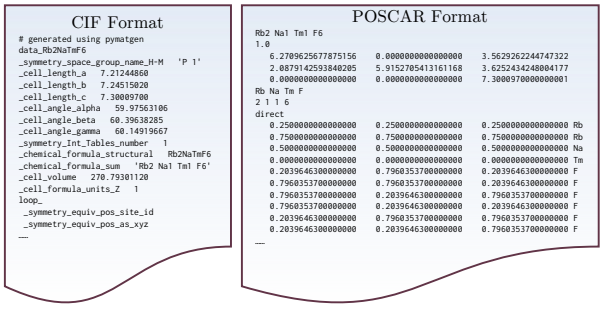

Figure S6: Structure string examples of CIF format and POSCAR format.

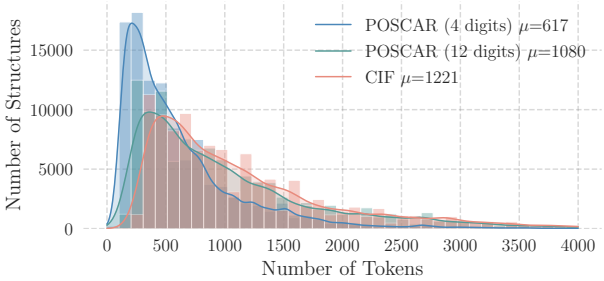

Figure S7: Token efficiency comparison under CIF formatting and POSCAR formatting for the precision of 4 and 12 decimal. μ indicate the mean of token lengths.

J Hyper-Parameter Studies

Reproduction Configuration	# Unique / # Total generated	$E_d < 0.1$eV/atom	$E_d < 0.03$ eV/atom
$1 \rightarrow 5$	56.5%	79.8%	56.4%
$2 \rightarrow 5$	72.3%	76.8%	56.5%
$2 \rightarrow 2$	86.3%	74.8%	54.3%
$5 \rightarrow 5$	92.7%	72.3%	47.3%
$5 \rightarrow 2$	95.5%	68.3%	46.1%

Table S11: Proportion of unique structures and their CHGNet-predicted metastability under varying reproduction configurations.

LLM Temperature	# Unique / # Total generated	$E_d < 0.1$ eV/atom	$E_d < 0.03$ eV/atom
0.95	72.3%	76.8%	56.5%
0.7	70.7%	75.4%	56.6%
0.5	70.7%	71.2%	51.4%
0.2	69.8%	70.3%	50.2%

Table S12: Proportion of unique structures and their CHGNet-predicted metastability with different LLM temperatures.

Reproduction parameters. Our training-free evolutionary framework significantly reduces hyperparameter sensitivity compared to traditional machine learning methods. The reproduction phase introduces several key hyper-parameters that influence LLMs' generation behavior and efficiency, including population size (K), context size (C), and children size (c). Our baseline configuration ($C = 2$, $c = 5$) leverages the Llama 3.1 (70B) model to achieve balanced performance, generating 72.29% unique structures while maintaining high stability rates.

Analysis of parent-to-children ratios reveals that increasing parent diversity ($C = 5$, $c = 2$) can enhance composition uniqueness of generated structures to 95.49%, though at the price of slight decrease in stability, as presented in Table S11. Conversely, results with single parent demonstrates that crossover between multiple parent structures is beneficial for maintaining structural diversity and stability in the generation process.

Overall, we believe that higher parent-to-children ratios can lead to better overall quality in generated structures.

Our analysis also reveals that larger population sizes K can maintain high stability and validity rates comparable to smaller populations. One potential benefit of increasing population size is the diversity introduced in the iteration process, which can alleviate the overpopulation of f-ele structures but also lead to higher compositional diversity. However, the increased diversity is offset by higher rates of structural duplication across iterations, suggesting earlier convergence may be needed. Our findings above enable application-specific optimization of the framework's parameters.

Model temperature. The temperature hyper-parameter controls sampling randomness in language models by scaling the logits before softmax transformation. Higher temperatures flatten the probability distribution, increasing sampling diversity, while lower temperatures concentrate probability mass on the most likely tokens. While temperature is commonly associated with model creativity, with higher temperatures generally producing slightly more novel outputs (Peeperkorn et al., 2024), this relationship remains an active area of research.

Crystal structure generation is a creative task that requires exploring diverse structural possibilities while maintaining physical validity. We employed an LLM inference temperature of 0.95 in our baseline experiments to facilitate broader structural exploration while maintaining reasonable generation stability. In Table S12, we present the metastability evaluated by CHGNet for structures generated with different LLM temperatures. At the temperature of 0.95, the LLM generated 76.81% metastable structures with $E_{\mathrm{d}} < 0.1$ eV/atom as evaluated by CHGNet. Reducing the temperature to 0.7 maintained robust performance, producing 75.38% metastable structures. Further lowering the temperature to 0.5 yields 71.18% metastable structures. If we choose $E_{\mathrm{d}} < 0.03$ eV/atom as the stability criterion, the percentage of qualifying structures at temperatures 0.95, 0.7, 0.5 and 0.2 are 56.5%, 56.6%, 51.4% and 50.2% respectively. The consistent high stability rates across temperature settings demonstrate the robustness of our pipeline to LLM hyper-parameter variations.

K Crystal Structure Prediction Examples.

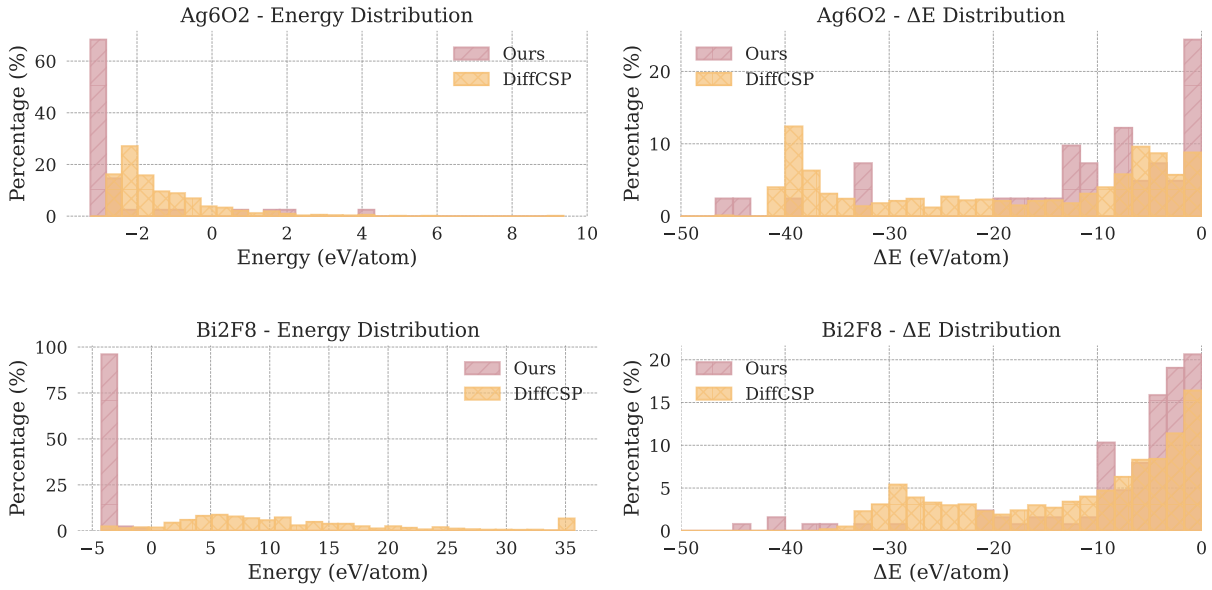

Figure S8: Energy and ΔE distributions comparing our LLM-generated structures versus DiffCSP predictions for Ag_6O_2 and Bi_2F_8 CSP tasks. LLM-generated structures show smaller $|\Delta E|$ values during relaxation than DiffCSP predictions.

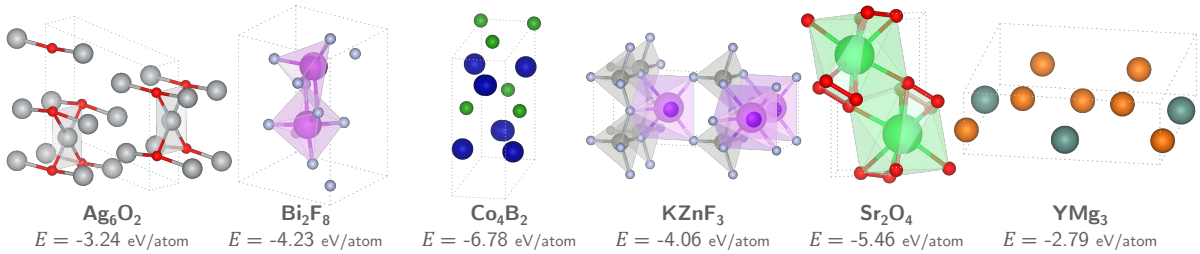

Figure S9: Representative CSP examples for six compositions (Ag_6O_2, Bi_2F_8, Co_4B_2, $KZnF_3$, Sr_2O_4, YMg_3) generated by MatLLMSearch.

We further evaluate MatLLMSearch on crystal structure prediction across multiple compositions. Crystal structure prediction fundamentally involves searching for the optimal atomic arrangement that minimizes the system's energy for a given composition.

For CSP task, we first apply compositional constraints to filter seed structures, and then execute MatLLMSearch for 10 iterations. This process enables the LLM to predict crystal structures by referencing from optimized structures with similar compositions.

To benchmark the effectiveness of our framework, we compare our results against structures generated and optimized by DiffCSP. We first used DiffCSP to sample 100 candidate structures for each composition. We then trained an energy predictor model on the MP-20 dataset for 1000 epochs to learn formation energy predictions. Then we applied the energy-guided optimization procedure to refine the structures with the trained energy model, generating 10 optimized variants for each initial structure. Orb-v3 (Rhodes et al., 2025) are employed to evaluate the energy of the relaxed structure from both sources.

MatLLMSearch successfully predicts structures for various compositions, including Ag_6O_2, Bi_2F_8, Co_4B_2, $KZnF_3$, Sr_2O_4, and YMg_3. Figure S9 presents representative examples of these predicted crystal structures, which achieve lower energies than the best structures predicted by DiffCSP.

To further evaluate the two approaches, we analyzed the energy and ΔE distributions of the generated structures. As shown in Figure S8, a large portion of structures predicted by DiffCSP experience substantial structural changes during relaxation, as indicated by large $|\Delta E|$ values. In contrast, our LLM-generated structures demonstrate superior initial stability, requiring minimal relaxation. This suggests that our initial configurations are already close to local energy minima.

L Details of Machine Learning Interatomic Potentials

A significant breakthrough in addressing computational cost challenges has emerged through the development of machine learning interatomic potentials (MLIPs) trained based on high-fidelity quantum mechanical calculations (e.g., DFT) (Batzner et al., 2022; Cheng, 2024; Du et al., 2023a;b; Liao et al., 2024; L'opez-Zorrilla et al., 2023; Yin et al., 2025; Zhang et al., 2021). In MLIPs, the total energy is expressed as a sum of atomic contributions, where each atom's energy depends on its local environment including the atomic coordinates and chemical species of neighboring atoms within a cutoff radius:

$$\hat{E} = \sum_{i}^{n} \phi(\{\vec{r}_j\}_i, \{C_j\}_i), \quad \hat{\boldsymbol{f}}_i = -\frac{\partial \hat{E}}{\partial \boldsymbol{r}_i}, \quad \boldsymbol{\sigma} = \frac{1}{V}\frac{\partial \hat{E}}{\partial \boldsymbol{\varepsilon}}. \tag{S1}$$

Here, ϕ is a learnable function that maps the set of position vectors $\{\vec{r}_j\}_i$ and chemical species $\{C_j\}_i$ of the neighboring atoms j to the energy contribution of atom i. The forces $\boldsymbol{f}_i$ and stress $\boldsymbol{\sigma}$ are calculated via auto-differentiation of the total energy with respect to the atomic Cartesian coordinates and strain. Recent advances have demonstrated that MLIPs, trained on extensive density functional theory (DFT) calculations accumulated over the past decade across diverse materials systems, exhibit remarkable transferability in performing atomistic simulations across various material and chemical systems. These broadly applicable

potentials are known as universal MLIPs (uMLIPs) (Batatia et al., 2023; Chen and Ong, 2022; Deng et al., 2023; Park et al., 2024). By leveraging uMLIPs as surrogate energy models, researchers can rapidly optimize crystal structures and obtain structure-energy relationships for assessing thermodynamic stability. By leveraging uMLIPs as surrogate energy models, one can rapidly optimize crystal structure and obtain the structure-energy relationships for assessing thermodynamic stability. Recent benchmark studies, including MACE (Batatia et al., 2023), DPA-1 (Zhang et al., 2024) and JMP (joint multi-domain pretraining) (Shoghi et al., 2024), have demonstrated the high accuracy of these uMLIPs in predicting crystal thermodynamical stability, particularly for industrial-scale implementations trained on millions of compounds and non-equilibrium atomic configurations (Barroso-Luque et al., 2024; Merchant et al., 2023; Yang et al., 2024a).

To accelerate the oracle function evaluation in the evolutionary iterations, we performed all structure relaxations with the `FIRE` optimizer (Bitzek et al., 2006) over the potential energy surface provided by CHGNet, where the atom positions, cell shape, and cell volume were optimized to reach converged interatomic forces of 0.1 eV/atom (Deng et al., 2023). The output energy prediction is directly compatible with the Materials Project phase diagrams with the `MaterialsProject2020Compatibility` (Wang et al., 2021).

M Failure Mode Analysis

We conduct a failure analysis of LLM-guided crystal structure generation to understand where and why structure generation fails. Using 100 prompts (2 parent structures each, 5 requested children per prompt) for three LLM configurations (DeepSeek-Reasoner with 16K-token for extended reasoning, DeepSeek-Chat standard 8K-token chat, and Llama-3.1-70B baseline), we track all 500 expected structures per model over multiple validation stages: LLM Generation, Parsing, Basic Validation, CHGNet Relaxation, and E_{d} Calculation.

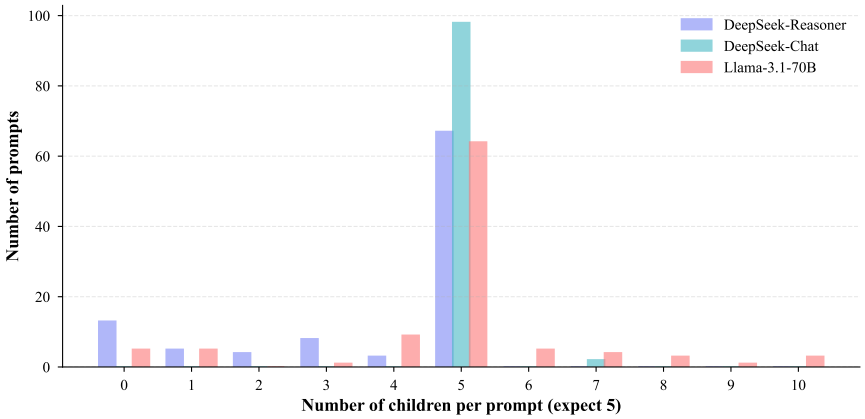

Figure S10: Distribution of children generated per prompt (before parsing and validation) for three LLM configurations.

Figure S10 shows the distribution of number of children generated per prompt with regex matching applied. **DeepSeek-Chat** demonstrates good instruction following to the 5-child requirement, while **Llama-3.1-70B** shows difficulty for complete responses. **DeepSeek-Reasoner** requires extra tokens for reasoning otherwise may lead to empty responses.

Format Error. Format errors in Table S13 includes JSON parsing errors when handling each response and POSCAR parsing errors when handling the POSCAR string for each of the childreninside the JSON response.

JSON Format Errors include empty responses and malformed JSON. DeepSeek-Chat shows best overal instruction following ability in formatting. DeepSeek-Reasoner can use up the tokens in reasoning and lead to empty responses. Llama more often generates malformed JSON. We apply regex matching to recover structures from malformed JSON, successfully extracting 405, 504, and 496 structures respectively.

Table S13: Failure mode breakdown (100 prompts × 5 children).

Category	DeepSeek-Reasoner	DeepSeek-Chat	Llama-3.1-70B
Generation Completeness (out of 100 prompts)			
Prompts with $\neq$ 5 children	33	2	36
JSON Format Error (out of 100 prompts)			
Empty responses	12	0	2
JSON parsing error	21	0	56
Total Regex Matched Structures	**405**	**504**	**496**
POSCAR parsing failures (after automatic fixing)	9	0	40
Total Parsed Structures	**396**	**504**	**456**
POSCAR Format Error (before automatic fixing, non-exclusive)			
Truncated strings (atom count mismatch)	15	19	237
Invalid numeric values	0	0	26
Invalid element tokens	0	0	20
Validation Failures (out of total parsed)			
Overlapping atoms (<0.5 Å)	0	13	125
Invalid stoichiometry	0	0	0
Charge imbalance	0	0	0
Volume/periodicity errors	0	0	0
Relaxation errors	0	0	3
E_{d} calculation errors	0	1	2
Valid Structures	**349**	**428**	**308**

POSCAR Format Errors are counted non-exclusively: truncated strings (atom count mismatches before fixing), invalid numeric values (e.g., "0.qlBay44"), and invalid element tokens (e.g., "Ue"). Truncation can occur mid-response (not only at the end), indicating LLM truncation behavior beyond token limits. Minor count mismatches are auto-corrected by aligning declared counts with coordinate lines. E.g. given a structure declaring "Lu 6 B 18 Rh 18" but providing only 14 B and 14 Rh coordinates, we adjust the atom counts to align with the actual coordinate lines.

Validation Failures. DeepSeek models show better performance in generating valid structures than Llama-3.1-70B, which more often generate structures with overlapping atoms or severe structual error that lead to relaxation or E_{d} calculation errors.

N Mutation & Crossover Analysis

To characterize genetic operations performed by LLMs during two-parent structure generation, we analyze the approximately 1K parsed valid structure from 100 prompts with 2 parent structures each. We classify operations into *mutation* (single-parent inheritance) and *crossover* (multi-parent recombination).

N.1 Mutation Analysis

1. **Same-Group Substitution:** Measures whether child elements belong to the same periodic group as replaced parent elements (e.g., $Dy_5RuI_7 \rightarrow Dy_5RuBr_7$ where I → Br within Group 17 halogens).
2. **Stoichiometry Preservation:** Evaluates exact reduced formula matching using pymatgen composition equality (e.g., $YbAlB_{14} \rightarrow ZrAlB_{14}$ preserves 1:1:14 ratio).
3. **Composition Similarity:** Quantifies element overlap via Jaccard index (set intersection/union) and Magpie feature-based cosine similarity (e.g., $Dy_2Sn_5Rh_3$ vs $Er_2Sn_5Rh_3$ yields Jaccard = 0.50, similarity = 0.993 due to shared Sn and Rh).
4. **Space Group Preservation:** Checks if child maintains parent's crystallographic space group number.
5. **Symmetry Preservation:** Evaluates preservation of both space group and Wyckoff positions.

6. **Lattice Similarity:** Assesses volume ratios and lattice parameter deviations (higher volume ratio indicates more identical cell volumes).

7. **Structural Matching:** Full structural matching using StructureMatcher with FrameworkComparator to detect exact geometric isomorphism regardless of element identity.

Observations. DeepSeek models in general demonstrate systematic application of crystallographic knowledge, supported by the high substitution rate of same-group elements as well as space group and symmetry preservation. All models exhibit minimal stoichiometry preservation and 0 structual match, preferring compositional and structural exploration over copying or minor modifications. Both DeepSeek models show slight preference for Parent 0 (first parent in the prompt).

N.2 Crossover Analysis

8. **Group-Based Recombination:** Identifies children incorporating unique elements from **both** parents (e.g., $AgRhF_6$ + $ZrAlAu_2$ → $AlRhAu_2$ where child takes Ag→Au substitution from Parent 0 and Al, Au elements from Parent 1, achieving true multi-parent crossover).

9. **Ratio Bounds:** Verifies whether child element fractions lie between parent fractions for shared elements (e.g., in $AlRhAu_2$, the Au fraction (0.50) lies within Parent 0's 0.00 and Parent 1's 0.50 range, demonstrating compositional interpolation).

10. **Density Bounds:** Assesses if child density falls within ±20% of parent density range.

Observations. DeepSeek-Chat achieves 31.0% group-based recombination rate, exceeding the other two models, suggesting better multi-parent exploration. All models follow a universal compositional interpolation constraint suggested by the perfect ratio bounding. DeepSeek models maintain 79% physically reasonable densities, while Llama shows higher average deviation indicating more often generation of geometrically unrealistic structures, which is accompanied by its higher composition error rate (Appendix M).

Table S14: Mutation and Crossover analysis results. Mutation analysis show per-parent inheritance metrics (Parent 0 and Parent 1). Crossover analysis show global multi-parent crossover metrics.

Category	DeepSeek-Reasoner		DeepSeek-Chat		Llama-3.1-70B	
	P0	**P1**	**P0**	**P1**	**P0**	**P1**
Mutation Analysis (Per-Parent Inheritance)						
1. Same-Group Elemental Substitution (%)	63.3	62.3	47.3	52.5	43.9	51.1
2. Stoichiometry Preservation (%)	0.0	0.0	1.3	0.6	2.2	1.7
3. Composition Similarity (Normalized)	0.821	0.787	0.826	0.802	0.774	0.770
4. Space Group Preservation (%)	53.1	41.8	39.8	32.3	18.9	27.8
5. Symmetry Preservation (%)	52.6	40.8	37.0	28.6	15.6	16.7
6. Lattice Similarity (Volume Ratio)	0.783	0.681	0.760	0.676	0.597	0.654
7. Structural Matching (%)	0.0	0.0	0.0	0.0	0.0	0.0
Crossover Analysis (Multi-Parent Operations)						
8. Group-Based Recombination (%)	18.2		**31.0**		14.4	
9. Ratio Bounds (%)	100.0		100.0		100.0	
10. Density Bounds (%)	79.0		79.1		52.2	
Parent Influence Analysis						
Dominant Parent Distribution (P0/P1)	58.7 / 41.3		58.9 / 41.1		47.8 / 52.2	